Engineering

Studia Universitatis Babeş-Bolyai
ENGINEERING

The Journal of the Faculty of Engineering at Reşiţa

Babeş-Bolyai University from Cluj-Napoca

Design of electrical power telemetering system using microcontroller device via GSM

Mohanad Abdulhamid

Abstract. *Traditionally, reading of energy meters is done by human operators who move from house to house collecting readings. This exercise requires huge labor operator numbers and a lot of time to achieve complete reading of meters in a particular area. This paper endeavors to do away with this problem by using a telemetering system. With this system, power can be measured from a remote site. To achieve this, readings from an energy meter on site are processed by a microcontroller device that then sends the energy consumption information to a Global System Mobile (GSM) module. The GSM module then sends this information using microwaves to a particular mobile subscriber who receives it in the form of an Short Message Service (SMS). The reading is also transmitted to a web based telemetering system through a server. In the remote site, a remote computer which can access the internet is able to obtain data from the server through the internet. The microcontroller is developed in such a way that it achieves communication between the energy meter and the particular server using Transmission Control Protocol(TCP) protocol. Software programs are also developed to facilitate transfer of data to the user at remote site. With the web based telemetering system connected to the internet, electrical energy measurements can be accessed globally. The efficiency of the transmission channel is important for the success of both SMS and web based telemetering systems.*

Keywords*: Telemetering system, remote sites, GSM*

1. Introduction

There is an impending rise in operations costs due to the expansion of customer base. Therefore, the need to implement a system that can cut down on the annual expenditures incurred as a result of the process of taking readings manually is crucial to the company. Moreover, this traditional manual reading process is

affected by the outside world whereby weather conditions, roads and transport conditions and other human factors play a huge role in the accessibility of the areas where measurements are to be taken. All these factors affect the efficiency of meter reading process. A telemetering system that is based on both internet and mobile phone communication systems is thus to be designed. This system addresses the above mentioned difficulties together with the issue of human error which is prone to occur when an operator is taking meter readings. The telemetering system combines computer network technology and the wireless communication technology to improve the efficiency and reliability of electricity meter reading process, reduce the operating cost of the power company, avoid human error and enabling optimized modern management of the company. With the introduction of digital technology, analogue electromechanical meters have been replaced by digital electronic meters. This digital technology provides a good platform for the implementation of Automatic Meter Reading (AMR) system as it involves using an electronic system [1, 2].

It must be noted that the concept of telemetering systems can be applied in many areas today, from meteorology to space science, water management, medicine and even military intelligence. However, this paper describes a telemetering system whose purpose is to measure electrical energy consumed by a particular consumer. Efficiency and reliability in retrieving the reading of a meter in the AMR system has proved to be a major challenge in the past. Many methods and technologies that use Power Line Carrier (PLC) communications, Supervisory and Data Acquisition (SCADA), Ethernet, internet Wi-Fi, Bluetooth, RF module, ZigBee have initially been developed to demonstrate the reliability, efficiency and effectiveness of AMR [3, 4, 5]. The above mentioned methods have proved to be either too expensive to implement and operate, they require complex setup of infrastructure as is the case of SCADA or are prone to error and reliability issues due to noise in the transmission line or weather condition. Rapid development of the GSM infrastructure in the past few decades has made wireless AMR system more reliable and possible. Therefore, focus will be aimed at the design of a system that will be able to take meter readings from a remote site and transmit these readings to a central station so that billing can be done by utilizing the GSM technology.

2. Methodology

In this section, the method used to implement the design is discussed using the following steps;
1. Measurement of energy consumed.
2. Transmission of the reading.
3. Reception of the reading.

To measure energy consumed, the current and voltage values are taken into consideration. The voltage value is taken as 240V, 50Hz which is the standard value of single phase voltage. This is the value of voltage that is be used throughout this paper.

Current drawn on the other hand keeps changing depending on the load connected to the meter. Therefore changes in current determine the amount of energy being consumed per hour. The power factor for low power consumers does not go low easily since the currents drawn are low.

It must be noted that the load used in this paper is a purely resistive load, therefore the voltage is in phase with the current. This means that the power factor will always be 1 as the cosine of 0 is 1. The waveform for power will therefore always be positive and never negative for this resistive load. This means that power will always be dissipated by the resistive load, never returned to the source as is the case with reactive loads. For the high power consumers, reactive loads are mostly connected. This affects the power factor value.

Once the reading has been taken, it is processed by a microcontroller in the meter then transmitted to a central station using GSM technology. The GSM module has a Subscriber Identification Module (SIM) card which facilitates this transmission process.

The reading is then received either through SMS or to a web application. In this paper, the readings are received through SMS and also via a web application. With this, real time access to the readings of the meter can be obtained. However, to minimize too much traffic in the servers for a real world practical implementation, the meter can be programmed to send meter readings after every 15 minutes.

2.1. Measurement of energy consumed

At the measuring point, current needs to be stepped down to low values before they are allowed to flow to the microcontroller without damaging the device. For high current values, a current transformer of say 1000/5A can be used. By this, the microcontroller can be programmed to recognize that when it reads a value of 5A, then it knows that this is 1000A, therefore the value of current that will be transmitted to the central station is 1000A. This is for the case of heavy consumers of electricity. The flow of data in the measuring unit is as follows;

1- Analog input signals: In this case the input signals to the measuring unit is the current.
2- The Analog to Digital converter (AD), is part of the meter measuring system which generates calibrated instantaneous digital value of the current from the analog input signals. For this paper, this ADC is in the Arduino microcontroller device.

2.1.1. Data preparation

The processor determines the mean digital values from the instantaneous values and current generated from the ADC. These mean values are averaged for one second in each case. The mean values in one second are active power, and current.

2.1.2. Signal processing

The microcontroller calculates the following measured quantities from the mean values provided by the signal processor;
- Mean active power in one second.
- Current in one second.

2.2. Simulation using Proteus software

A simulation of our work is carried out using Proteus software. This is carried out using the following set of components;
1. Resistors.
2. A liquid-crystal display (LCD).
3. Power supply.
4. A load of 240 Ohms.
5. An Arduino Uno.
6. Capacitors.
7. ACS712T Hall Effect current sensor.

2.2.1. Current measurement

Current measurement is achieved using the ACS712T (20A). This current sensor is connected in series with the load to facilitate current measurement. The ACS712T is a sensing device that provides an economical and precise way of sensing AC current passing through it using the hall-effect principle.

The ACS712T is based on hall-effect. According to this principle, when a current carrying conductor is placed in a magnetic field, a voltage is generated across its edges perpendicular to the directions of both the current and the magnetic field.

Due to the presence of Lorentz force (force due to the combination of the magnetic and the electric forces), the current distribution is no longer across the hall element and thus a potential difference is created across the edges perpendicular to the directions of both the currents and the field. This voltage is called the hall voltage.

The ACS712 device consists of a precise, low-offset, linear hall sensor circuit with a copper conduction path that is located near the surface of the die. When current is applied through the copper conductor, a magnetic field is generated and this is sensed by the hall-element. The strength of the magnetic field is proportional to the magnitude of the current through the conductor. The signal conditioner and filter circuit which are on the chip stabilize the induced hall voltage to appropriate level so that it can be measured through an ADC channel of the microcontroller.

Terminals of the conduction path are completely electrically isolated from the sensor leads. The ACS712T therefore eliminates the risk of damaging the current monitoring circuit as a result of high voltage on the conduction side.

Since our research involves use of low frequency AC, 50Hz, an RC filter circuit is added at the output of the ACS712 device. This is useful to improve the signal to noise ratio. It must be noted that no resistor is connected in the RC filter, this is because the ACS712 contains internal resistor connected to the output of the on-chip signal amplifier. Therefore simple addition of an external capacitor between the filter pin and the ground would suffice. Since the bandwidth decreases with increasing capacitance, the datasheet of the ACS712 recommends to use 1nF for the capacitor to reduce noise under normal condition.

2.2.2. Output of the ACS712

The ACS712-05B can measure current up to ±20A and provides an output sensitivity of 100mV/A (at +5V power supply). This means that for every 1A increase in the current through the conductor in the positive direction, the output voltage also rises by 100mV. At zero current, the output voltage is half of the supply voltage (Vcc/2). The voltage at zero current is found to be 2.4V when Proteus software is used in simulation. This value is close to the half way value of 2.5V. This is the offset of the ACS 712 current sensor.

The ACS712 provides a ratio output in that the zero output current and the device sensitivity are both proportional to the supply voltage, V_{CC}. This feature is useful since the ACS712 is used with an ADC and A/D conversion depends on the stability if the reference voltage used in the ADC operation. The ACS712 has a voltage stabilizer which makes the output to be constant at 2.5V.

Care must however be taken when working with the ACS712 sensor as it is susceptible to stray magnet fields. The following conditions could affect the value of current being sensed;

1. Stray field resulting from current flowing in a printed circuit board or an external current carrying conductor that is close to the ACS712.
2. External current carrying conductor is on the same plane as the current sensor.

Figure 1 below shows the absolute current error (in A) versus the distance of the hall element from the primary conductor (in mm) for different current values, in A.
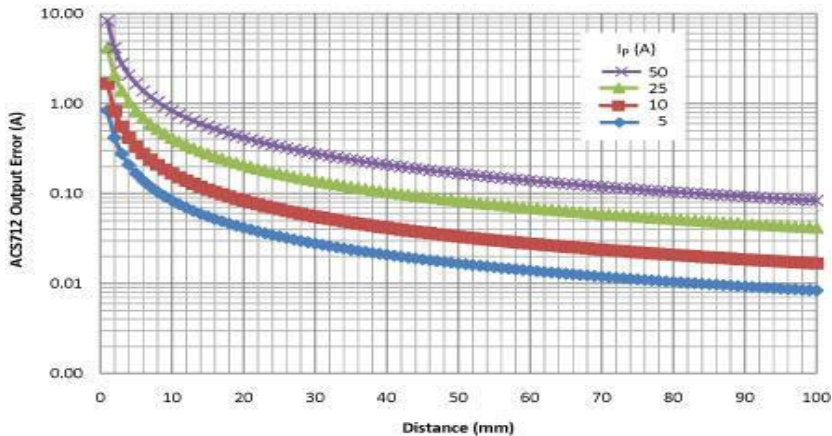

Figure 1. Absolute Output signal error versus distance between the hall element and the External PCB conductor at various levels of current

Shielding must therefore be done on the hall element to prevent stray magnetic fields from interfering with the measurements being taken.

2.3. Time measurement

Time is important since energy consumed is directly proportional to the period of time that the load is connected to the supply and is drawing current.

To measure time, no external hardware is needed as the Arduino has an inbuilt timer. The millis () function is used in the code. What this function does is that it returns the number of milliseconds since the board begin to run the program. Therefore from the instant the program is run, time starts to be taken into consideration.

With this functionality, the meter will give real time energy consumption readings which can then be transmitted.

2.4. Data processing

By scanning the mean values per second (active power, voltage, frequency, power factor), the microprocessor forms related measured quantities. This is done by the ATmega 328 on the Arduino Uno board. These measured quantities are then displayed on an LCD display. A remote readout is also ready to be carried out at this point.

8

2.4.1. The Arduino Uno R3 microcontroller unit

The Arduino Uno is used to process the data readings and send them to the GSM module for transmission. The Arduino is a microcontroller board based on the ATmega328P. It has 14 digital input/output pins; 6 of which can be used as *Pulse Width Modulation* (PWM) outputs. It also has 6 analog inputs, a 16MHz quartz crystal, a *Universal Serial Bus (*USB) connection, a power jack, an In-Circuit Serial Programming (ICSP) header, and a reset button.

2.5. Transmission of measurements

The GSM module is interfaced with the microcontroller as shown in Fig.2 to ensure exchange of information on the measured quantities. In this case, the GSM module obtains information on the measured quantities from the microcontroller. A serial communication at some predetermined baud rate ensures communication between these two devices.

Figure 2. Interfacing of the GSM module and the microcontroller.

The measuring unit has a unique serial number that makes it possible to interrogate it specifically and obtain all the information on the quantities being measured. This therefore provides real time access to measured quantities.

The GSM module used is the SIM 900A. This is an ultra-compact and reliable wireless module made by SIMcom that works well with the Arduino microcontroller unit. It is a complete dual-band GSM/GPRS module in the Surface Mount Technology (SMT) type and allows us to benefit from the small dimensions and cost-effective solutions. It has SMT pads and uses a single-chip processor integrating ARM926EJ-S. The module delivers the GSM/GPRS 900/1800MHz performance for voice, SMS, data and fax with low power consumption. With a small configuration of 24mm x 24mm x 3mm, the module can fit many space requirements for our applications.

2.5.1. Sending data using SMS

After calculations of power and energy consumed done by the microcontroller, the data is now ready to be sent to the central station.

Here, code is also written to make the SIM900A start operating in SMS text mode hence make it possible for the GSM module to send SMS to the mobile phone subscriber that is also specified. It must be noted that GSM module has two modes of operation, the SMS text mode and the SMS Protocol data Unit (PDU) mode. In SMS text mode, the SMSs are represented as readable text while in PDU mode, all SMS messages are represented as binary strings encoded in hexadecimal characters.

Within the code, delays of several seconds are used after every command to give the GSM module enough time to interpret and respond to the commands.

In specifying the SMS content being sent, the program is set such that it called voltage, current and energy outputs from the code used to measure the energy parameters. These outputs are then sent to the specified subscriber as indicated in the code. The received SMS has data on energy consumed, voltage and current values.

2.5.2. Sending data to a web application

ThingSpeak is also used to show the results of energy consumption. ThingSpeak is an open source Internet of Things (IoT) web application that can store and retrieve data using Hypertext Transfer Protocol (HTTP) and TCP protocols over the internet or through local area network. It enables sensor logging applications for various kinds of sensors. With the web application, values of energy consumed in KWh are recorded online on a real time basis. This data can be displayed in various ways. The one used in this case is a chart displaying energy consumed on the y-axis and the time of the day when the data is collected on the x-axis. This web application is advantageous because once the data is uploaded, it is stored in a database and can be queried on a specific date range for the purpose of analysis or whatever the user wants it for.

To upload energy consumption readings, a program is written for making the GSM module to transmit the measurements of energy consumed in KWh to ThingSpeak web application in real time.

In the code, a command that sought information about the registration status and access technology of the serving cell is written. This is important as it checks whether the SIM card can actually perform the tasks needed. These tasks include GPRS capability. Code that also attaches packet service is written, then the GSM module is set for single IP connection and the Access Point Name (APN) set according to the Internet Service Provider (ISP) used. For our case, we use Airtel APN. The GPRS is then enabled and an IP address obtained through the appropriate AT

command as shown in the code. A TCP connection is then started to a remote address which for this case is api.thingspeak.com, the web application that would display the results remotely.

With the above settings made, data on electrical energy consumption is sent to the web application using the specified Attention (AT) command. The data is then ready for analysis from the web application.

2.6. Final design schematic diagram

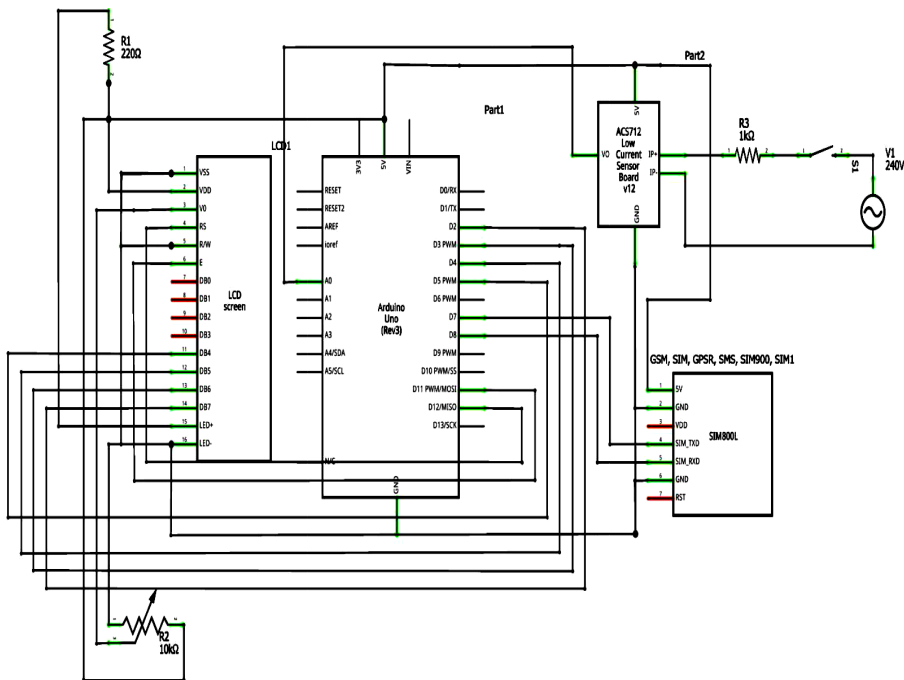The final design diagram is shown in Fig.3.

Figure 3. Final design

3. Results

The results in this paper are the measured quantities of current and energy consumed when different loads are connected. It is seen that a larger load draws more current and consequently consumed more energy. This phenomenon can be seen from the chart in Figure 4 showing energy consumption when different loads are connected.
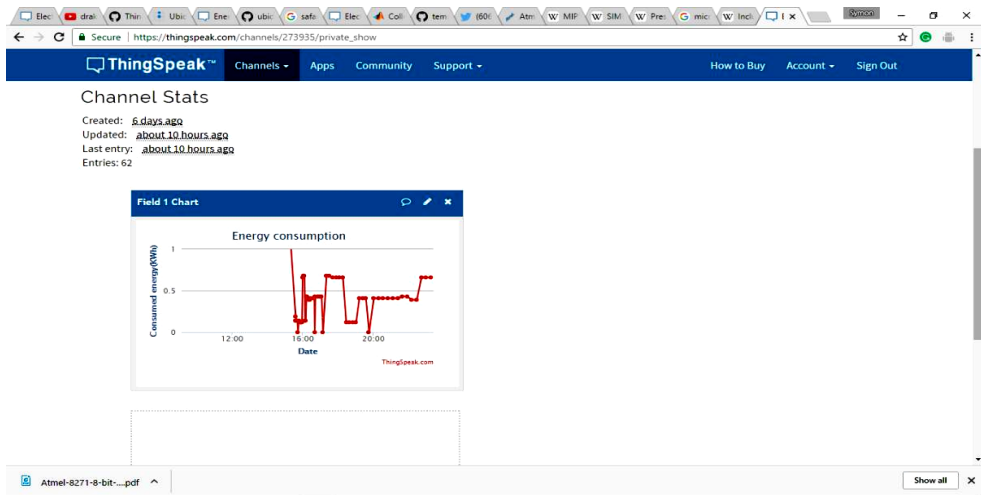
Figure 4. Chart showing energy consumption

From Fig.4, it can be seen that there is a variation on the energy consumed with time. The 100W load which is the largest load used for this paper, consumed an average of 0.66KWh. This can be seen on the chart at about 1800hrs while the 60W load consumption is at about 0.41KWh which can be seen on the chart at 2000hrs. It can also be observed that the energy consumed is fairly constant for any particular load. This means that the current drawn did not vary immensely for one connected load which is what is expected. In the calculation of energy consumed, the period of time for which the bulb is ON is 5hours. This is so as to ensure that the value of energy consumed is significantly larger for the purpose of recording the consumption.

From calculation;

$$P = V \times I$$

For the 100W load, with the supply voltage at 240V, 50Hz, the calculated value of current that should be drawn ignoring any losses is as follows;

$$I = P/V = 100W/240V = 0.4167A$$

The measured current was found to be 0.55A. The difference between these two values is found to be 0.133A. The 60W load on the other hand has the following calculated values of current;

$$I = 60W/240V = 0.25A$$

This value is slightly different from the measured value of 0.35A. However it must be noted that the reading recorded when there is no current flowing is actually

0.12A, meaning that the ACS712T exhibits a zero error of 0.12A. Taking this error into consideration this, the value of current being drawn by the 100W load is

$$0.55 - 0.12 = 0.43A$$

This makes the percentage error to be;

[(Calculated value - Measured value)/Calculated value] $\times 100$

$$= [(0.4167 - 0.43)/ 0.4167] \times 100 = 3.2\%$$

While for the 60W load, the actual current measured is 0.35-0.12= 0.23A and percentage error for this value is therefore 8%.

The small differences in these values are as a result of errors introduced by a difference in the supply voltage. This voltage is assumed to be constantly at 240V. This might not be the case at all times as this value could go down slightly thereby contributing to the difference in the two values of the currents.

As mentioned earlier, the values of energy consumed recorded on this particular chart are for a load that has been connected to the power supply for a period of 5hours.

For cumulative energy meter recording, the chart shown in Fig.5 shows measured energy consumption for a connected load of 60W over a period of 9 hours.
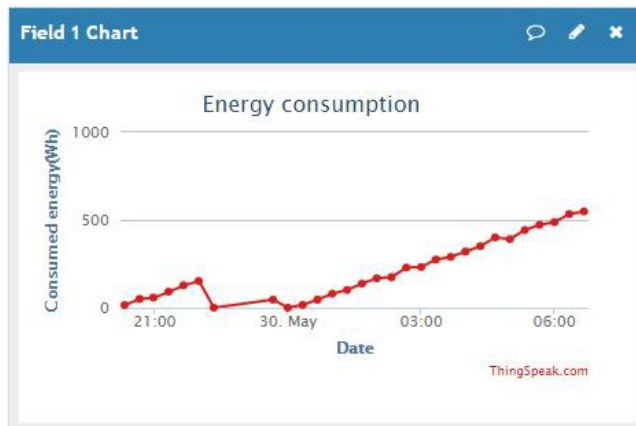

Figure 5. Chart showing meter reading as seen from the web application

From the chart in Fig.5, it is observed that between midnight and 6am, the energy consumed increased steadily. This is because between this periods of time, the 60W load is connected to the supply and therefore

consumes a total of 524Wh or 0.524KWh. The readings recorded on the web application can be seen from Table 1. It is also seen that the load is turned off at around 1927hrs and at 2052hrs. The utility company officer at the central location, must take this effect consideration so that when calculating the energy consumed for this particular consumer, only the peak values are summed.

The total consumption according to the chart is therefore 1217.11Wh or 1.217KWh as seen in Table 1.

For all these values of energy consumed, the current measured is found to be 0.35A. When you consider the 0.12A zero error value, then the actual value of current is 0.23A. Comparing this to the calculated current value of 0.25A, we get that the two are very close.

Table 1. Meter Readings on Web application at intervals of 10 Minutes

Created_at	Entry_id	Consumption (Wh)
2017-05-29 18:45:59 UTC	113	127.95
2017-05-29 19:08:01 UTC	114	152.31
2017-05-29 19:27:56 UTC	115	0.16
2017-05-29 19:38:57 UTC	116	15.37
2017-05-29 20:44:44 UTC	117	46.05
2017-05-29 20:52:47 UTC	118	0.05
2017-05-29 20:56:31 UTC	119	0.05
2017-05-29 21:00:26 UTC	120	0.05
2017-05-29 21:03:44 UTC	121	0.05
2017-05-29 21:09:09 UTC	122	0.15
2017-05-29 21:20:11 UTC	123	16.17
2017-05-29 21:31:13 UTC	124	32.16
2017-05-29 21:42:14 UTC	125	45.87
2017-05-29 21:53:16 UTC	126	58.05
2017-05-29 22:04:18 UTC	127	80.16
2017-05-29 22:15:20 UTC	128	91.57
2017-05-29 22:26:22 UTC	129	101.47
2017-05-29 22:37:23 UTC	130	122.04
2017-05-29 22:48:26 UTC	131	137.3
2017-05-29 22:59:27 UTC	132	152.54
2017-05-29 23:10:29 UTC	133	167.77

Created_at	Entry_id	Consumption (Wh)
2017-05-29 23:21:30 UTC	134	173.86
2017-05-29 23:32:32 UTC	135	198.25
2017-05-29 23:54:36 UTC	136	228.72
2017-05-30 00:05:38 UTC	137	231.75
2017-05-30 00:16:39 UTC	138	259.19
2017-05-30 00:27:41 UTC	139	274.42
2017-05-30 00:38:43 UTC	140	304.17
2017-05-30 00:49:45 UTC	141	289.67
2017-05-30 01:00:47 UTC	142	320.15
2017-05-30 01:11:48 UTC	143	335.39
2017-05-30 01:22:50 UTC	144	350.62
2017-05-30 01:33:52 UTC	145	365.86
2017-05-30 01:44:54 UTC	146	400.15
2017-05-30 01:55:55 UTC	147	396.33
2017-05-30 02:06:57 UTC	148	390.99
2017-05-30 02:17:59 UTC	149	426.82
2017-05-30 02:29:15 UTC	150	442.06
2017-05-30 02:51:09 UTC	151	472.53
2017-05-30 03:02:06 UTC	152	487.77
2017-05-30 03:13:08 UTC	153	528.15
2017-05-30 03:35:12 UTC	154	533.47
2017-05-30 03:46:14 UTC	155	548.71
2017-05-30 03:57:15 UTC	156	958.74
TOTAL ENERGY CONSUMED		1217.11

The readings are also obtained remotely through SMS. The photo in Figure 6 shows meter readings as received through SMS.

This image best depicts the zero error that is talked about earlier. It is seen from the first reading that no load is connected yet, the recorded current value is 0.12A. In the code, an if statement is written so that if the value of current is less than 0.12A, then the meter would take this value of current as zero. Hence the reading of KWh above is 0.00. This would therefore take care of the problem where the meter records energy consumption in a case where no load is consuming any energy. The resistance of the connecting copper conductors may have contributed to the flow of this current when the load is off.
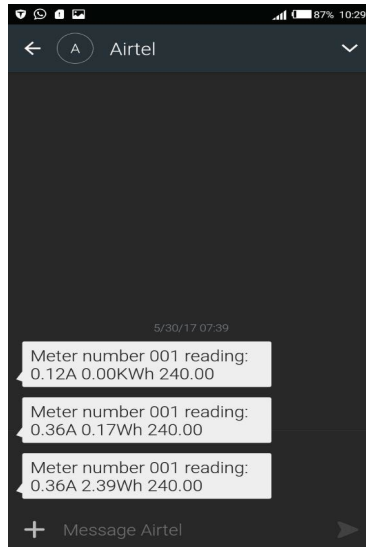
Figure 6. Screenshot of a meter reading as received by SMS

4. Conclusion

The telemetering system was designed using the Arduino Uno which has Atmega 328P microcontroller as the processing unit. An ACS712T (20A) current sensor was used as the current measuring unit while the GSM SIM 900A was the transmitting unit. The loads used were a 100W and 60W bulbs. Simulations were done on Proteus to test the working of the measuring unit with Arduino Uno. As demonstrated, real time measurements of current and energy consumption were transmitted using the GSM module to a mobile subscriber number and data on energy consumed uploaded to a web application called ThingSpeak.com. With this the objectives of the paper were fulfilled. The zero error exhibited from the measuring unit was taken into consideration while taking calculations of current drawn by the loads. Through this, it was seen that the percentage error of the measurements was quite small.

References

1   Jacob K., Ramanujam V., Telemetry in power systems, *IETE Journal of Research,* 29(8), 1983, pp. 373-377.
2   Jamil M., Munir F., Khan A., Mirza A., *Telemetering billing system for spatially distributed electrical power clients*, IEEE Conference of E-Tech, 2004, Pakistan.
3   Ratniyomchai T., Jaithong U., Kulworawanichpong T., Power line carrier for power telemetering, *International Journal of Electrical and Computer Engineering*, 2011, 5(8), pp. 975-978,
4   Önler E., Soner C., Aytaç M., İlker H., Development of telemetry system for electric powered vehicle, *International Journal of Current Research*, 8(9), 2016, pp. 38715-38719.
5.   Harris S., Kannan A, GSM based smart energy meter with optocoupler, *International Research Journal of Modernization in Engineering Technology and Science*, 4(9), 2022, pp 2579-2585.

Address:

- Mohanad Abdulhamid, Al-hikma University, Baghdad, Iraq,
  moh1hamid@yahoo.com

Determining the temperature using natural frequencies and artificial intelligence

Alexandra-Teodora Aman, Zeno-Iosif Praisach*, Gilbert-Rainer Gillich, Vasile Cătălin Rusu

Abstract. *The current paper explores a novel approach for determining temperature variations by integrating the modal parameters and AI techniques. The research focuses on the development of a comprehensive dataset for training an AI model encompassing an analytical method that considers thermal conditions and natural frequencies. Traditional methods of temperature measurement, like infrared and platinum resistance thermometers, often face limitations in terms of accuracy, especially in complex or dynamic environments having an uncertainty of ±3.6 °C [1], respectively ±0.2 °C [2]. In this study, we propose a methodology that harnesses the inherent relationship between axial loads caused by temperature variations and the change in natural frequencies of a double clamped steel beam. The measured natural frequency data is collected and fed into the AI model, specifically, for a robust temperature estimation, obtaining a maximum predicted temperature deviation of 0.386 °C.*

Keywords*: temperature, natural frequency, artificial intelligence, finite element method, thermal condition*

1. Introduction

Environmental variations can modify the modal characteristics of structures [3], which can result in a correlation between the natural frequencies and temperature. The effect of temperature is considered by most researchers as the most significant in the change in the dynamic behavior of the structure rigidly fixed at the ends [4 - 6]. Its effect on the natural frequencies of metallic structures is presented in [7, 8]. In the work [9], a study was carried out in which the influence of the temperature upon the natural frequencies of a simply supported reinforced concrete beam is analyzed, and the effect of the temperature variation is quantified.

In papers [10, 11] the authors found that the variations in natural frequencies caused by the temperature changes were comprised of between 4.7 and 6.6 %, which was more significant than the changes caused by an artificial cut.

The current study proposes a machine-learning model that can predict environmental temperature changes by considering the natural frequency shift due to temperature changes in double-clamped steel beams. The changes in the eigenfrequencies are determined by the axial forces developed by the fixed expanding structure [12]. The considered structure is a double-clamped steel beam, with its properties denoted in Table 1.

Table 1. Physical-mechanical properties of the material

Mass density ρ [kg/m³]	Young modulus E [N/m²]	Poisson ratio υ [-]	Thermal expansion coefficient α [mm/°C]
7850	$2.06 \cdot 10^{11}$	0.28	0.015

The considered beam's geometry and dimensions in mm are presented in Fig 1.
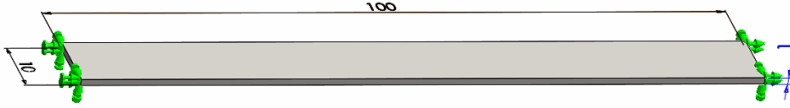

Figure 1. Double-clamped beam

By considering a reference temperature T_{ref} which is increased with ΔT, the internal force is given by [13]:

$$P(T) = \alpha \cdot E \cdot A \cdot \Delta T \tag{1}$$

where A is the cross-section of the beam, E is the elasticity modulus and α is the thermal expansion coefficient.

The characteristic equation for a beam fixed at both ends is [10]:

$$\zeta \sin \zeta + 2 \cos \zeta - 2 = 0 \tag{2}$$

The critical forces P_{cr} and critical temperature T_{cr} can be found as [10]:

$$P_{cr-i} = \frac{\zeta_i^2 E \cdot I}{L^2} \tag{3}$$

and

$$T_{cr-i} = T_{ref} + \Delta T_{cr} = T_{ref} + \frac{P_{cr-i}}{\alpha \cdot E \cdot A} \tag{4}$$

By applying the transcendental Equation (5), the values for the first six bending vibration modes are obtained [10]:

$$1 + \cos \lambda \cdot \cosh \lambda = 0 \tag{5}$$

For a compression load scenario with fixed-fixed ends, when ζ_i is not equal to λ_i, the natural frequencies can be calculated using Equation (6) [10].

$$f_i(P) = f_{ref-i} \sqrt{1 - \frac{P}{P_{cr-i}}} \tag{6}$$

The mathematical equation representing the frequency change due to temperature variation is derived by inserting Equations (1) and (3) into Equation (6), resulting in [10]:

$$f_i(T) = f_{ref-i} \sqrt{1 - \frac{\alpha A(T - T_{ref})L^2}{I\zeta_i^2}} = f_{ref-i} \cdot \kappa_i(T) \tag{7}$$

where $k_i(T)$ is the temperature adjustment coefficient.

For a reference temperature T_{ref}, the first six buckling eigenvalues ζ_i, the bending vibration eigenvalues λ_i critical force P_{cr}, and critical temperature T_{cr} values for the double-clamped beam are shown in Table 2.

Table 2. The first six eigenvalues, critical forces, and temperatures

Buckling mode i	Eigenvalue ζ_i	Eigenvalue λ_i	Critical force P_{cr-i} [N]	Critical temperature T_{cr-i} [°C]
1	6.283185307	4.7300407	6.777128355	22.28607549
2	8.986818916	7.8532046	1386.430028	80.52385089
3	12.56637061	10.9956078	2710.851342	136.4301959
4	15.45050367	14.1371654	4097.993428	194.9841042
5	18.84955592	17.2787596	6099.41552	279.4679409
6	21.80824332	20.4203522	8164.457682	366.6373019

Applying the described method, a database consisting of the Relative Frequency Shifts (RFS's) is generated using Equation 8, by considering the reference temperature T_{ref}=22°C and the iterative temperature increase of Δt=2°C, until T_{final}=50° thus obtaining 141 scenarios including the reference temperature where the RFS values for all modes are zero.

$$RFS_i = \frac{f_{ref-i} - f_i(T)}{f_{ref-i}} \tag{8}$$

2. Training the ANN

A robust ANN for predictive analysis is modeled using the nntool with Bayesian regularization through MATLAB software with a focus on predicting temperatures using the RFS data which was inserted as input [11]. The Bayesian regularization approach is used to prevent the overfitting phenomenon and to enhance the network's ability to better generalize on new data. The ANN is composed of two hidden layers, each containing 30 neurons, with its architecture presented in Figure 2.
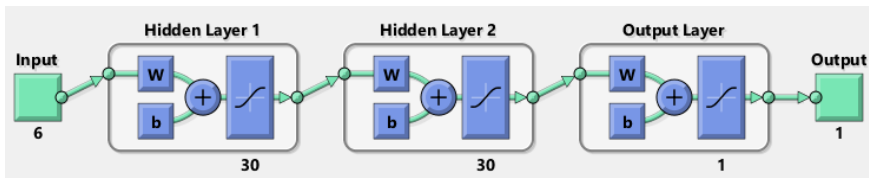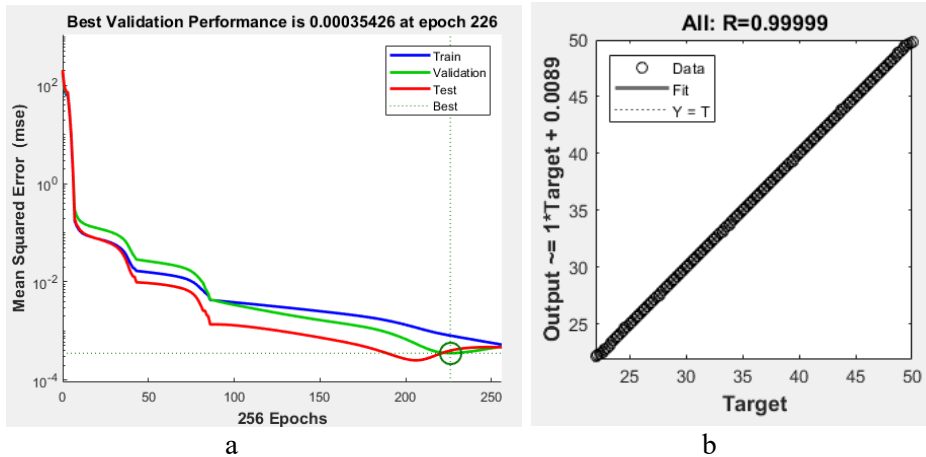

Figure 2. Network architecture

a

b

Figure 3. Network performance plots

21

Evaluating the trained neural network's performance involves employing visualization tools such as performance curves (Figure 3a) and regression plots (Figure 3b). 70 % of the data is used for training, 15% for validation, and 15% for testing. The performance curves offer a dynamic view of the network's learning process, typically accuracy or error rate, plotted against the number of training iterations. Regression plots, on the other hand, visually compare predicted values against actual data points.

3. Evaluating the accuracy of the ANN

In the testing phase of the Artificial Neural Network (ANN), SolidWorks frequency simulations were employed to model the necessary conditions for a double-clamped beam model, as illustrated in Figure 1. The material properties were defined using plain carbon steel from the library. A fine solid mesh having 20111 nodes and 11598 total elements is applied, and the analysis is run across various thermal scenarios, simulating different temperatures affecting the beam coupled with the modal analysis, with an example illustrated in Figure 4. All defined scenarios are presented in Table 3. During each simulation, the natural frequencies for the first six bending vibration modes were recorded, starting from the reference temperature T_{ref}=22°C and continuing with other beam temperatures.
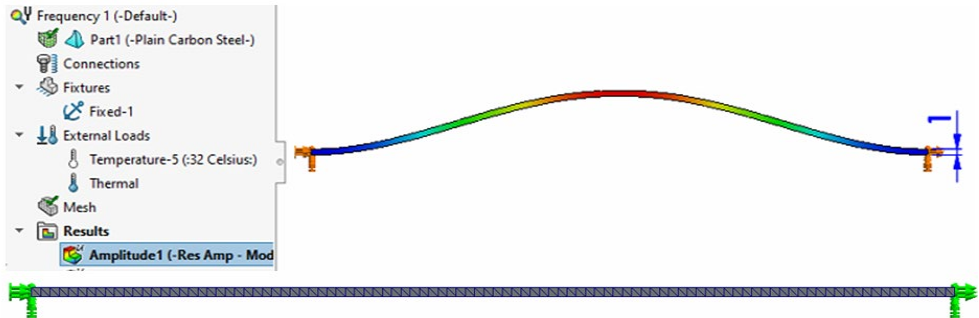

Figure 4. Frequency analysis and geometry meshing

4. Results and discussions

These frequency values served as inputs for calculating the Relative Frequency Shifts (RFSs) using Equation 8. The RFS values were utilized as testing data for the ANN. For each simulation scenario, the predicted temperatures were compared with the known temperatures obtained from SolidWorks frequency simulations. By applying several thermal conditions, the ANN's capability to accurately predict temperatures demonstrates its ability to generalize. The obtained results are presented in Table 3.

Table 3. Temperature scenarios and obtained results

Scen no.	Known temperature [°C]	Predicted temperature [°C]	Temp. difference
1	28	28.0000	0
2	22.5	22.4421	0.0579
3	23.2	23.1049	0.0951
4	23.9	23.7569	0.1431
5	33.5	33.7700	-0.270
6	42.1	41.7142	0.3858

Based on the obtained results, with errors not exceeding 0.92 %, the ANN demonstrates that it can predict the temperature with high accuracy, even when it is trained by using analytical data and tested with new data generated by simulations, thus having to deal with new RFS values that are not fitting 100% with the calculated ones, as illustrated in Figure 5 for cases 6 and 2.
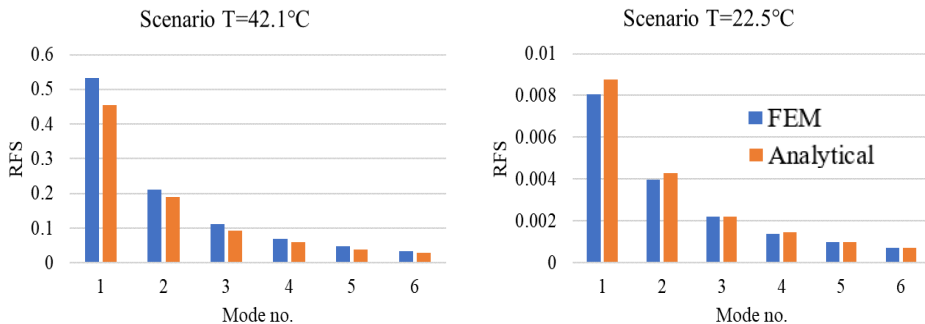

Figure 5. Comparison of calculated and FEM RFS values for scenarios 6 and 2

5. Conclusion

The current paper presents novel research for predicting the temperature by using modal parameters of structures such as the natural frequencies, coupled with intelligent learning models developed through specialized software.

An earlier developed mathematical method is used for generating the necessary training data to develop an ANN model that can predict the temperature by calculating thermal adjustment coefficients and calculating the RFS input data.

The ANN model is tested with new data, employing FEM simulations, and the results obtained illustrate a maximum deviation of 0.3858 °C, thus obtaining a temperature reading of high accuracy. Even if the accuracy does not reach that of liquid-in-glass thermometers, that can achieve a measurement uncertainty of ±0.01 °C [2], the experiment demonstrated that achieving even better temperature accuracy is feasible through the careful adjustment of hyperparameters in the Artificial Neural Network (ANN) and the utilization of a substantially larger training dataset.

The findings suggest that investing time and resources into optimizing the hyperparameters of the ANN, coupled with the acquisition of an extensive and varied dataset, can lead to significant improvements in temperature accuracy. This approach holds promise for applications where precise temperature measurements are critical, offering a pathway for enhancing the reliability and performance of temperature prediction models.

References

1   Shuanglong C., Bojun S., Xiaogang S., A method for improving temperature measurement accuracy on an infrared thermometer for the ambient temperature field, *Review of Scientific Instruments*, 91, 054903, 2020.
2   BS1041-2.1:1985 Temperature Measurement- Part 2: Expansion thermometers. Section 2.1 Guide to selection and use of liquid-in-glass thermometers.
3   Cornwell P., Farrar C.R., Doebling S.W., Sohn H., Environmental variability of modal properties, *Experimental Techniques*, 23(6), 1999, pp. 45–48.
4   Tufoi M., Gillich G.R., Praisach Z.I., Iancu V., Furdui H., About the influence of temperature changes on the natural frequencies of clamped-clamped euler-bernoulli beams, *Romanian Journal of Acoustics and Vibration*, 11, 2014, pp. 84-87.
5   Azadi M., Free and forced vibration analysis of FG beam considering temperature dependency of material properties, *Journal of Mechanical Science and Technology*, 25(1), 2011, pp. 69-80.

6   Soo Lon Wah W., Xia Y., Elimination of outlier measurements for damage detection of structures under changing environmental conditions, *Structural Health Monitoring*, 571(1), 2011.

7   Liu H., Wang X., Jiao Y., Effect of temperature variation on the modal frequency of reinforced concrete slab and beam in cold regions, *Shock and Vibration*, 6, 2016, pp. 1-17.

8   Yijiang M., Guoping C., Modal analysis of a rectangular variable cross-section beam with multiple cracks under different temperatures, *Journal of Vibroengineering*, 18., 2016, pp. 3078-3088, 10.21595/jve.2016.16676.

9   Cai Y., Zhang K., Ye Z., Liu C., Lu K., Wang L., Influence of Temperature on the Natural Vibration Characteristics of Simply Supported Reinforced Concrete Beam, *Sensors (Basel)*, 21(12), 2016, pp. 4242, doi: 10.3390/s21124242. PMID: 34205726; PMCID: PMC8234513.

10   Sohn H., Dzwonczyk M., Straser E.G., Kiremidjian A. S., Law K., Meng T., An experimental study of temperature effect on modal parameters of the Alamosa Canyon Bridge, *Earthquake Engineering and Structural Dynamics*, 28(7-8), 1999, pp. 879–897.

11   Farrar C. R., Doebling S.W., Cornwell P. J., Straser E. G., Variability of modal parameters measured on the Alamosa Canyon bridge," in *Proceedings of the 15th International Modal Analysis Conference (IMAC '97)*, pp. 257–263, Orlando, Fla, USA, February 1997.

12   Khangamlung K., Muhammad A.K., Kamran A.K., Characterising modal behaviour of a cantilever beam at different heating rates for isothermal conditions, *Applied Sciences*, 11, 2021, p. 11104, https://doi.org/10.3390/app11104375biographies

13   Gillich G.R., Furdui H., Wahab M.A., Korka Z.I., A robust damage detection method based on multi-modal analysis in variable temperature conditions, *Mechanical Systems and Signal Processing*, 115, 2019, pp. 361–379, https://doi.org/10.1016/j.ymssp.2018.05.037

14   Gillich N., Tufisi C., Sacarea C., Rusu C.V., Gillich G.R., Praisach Z.I., Ardeljan M., Beam Damage Assessment Using Natural Frequency Shift and Machine Learning, *Sensors,* 2022, 22(3):1118.

Addresses:

- Ph.D. Stud. Eng. Alexandra-Teodora Aman, Doctoral School of Engineering, Babes-Bolyai University, Cluj-Napoca, Romania, Faculty of Engineering, Piaţa Traian Vuia, nr. 1-4, 320085, Reşiţa, Romania alexandra.aman@ubbcluj.ro

- Lect. Ph.D. Eng. Zeno Iosif Praisach, Department of Engineering Science, Babeș-Bolyai University, Cluj-Napoca, Romania, Faculty of Engineering, Piața Traian Vuia, nr. 1-4, 320085, Reşiţa, Romania zeno.praisach@ubbcluj.ro ([*]*corresponding author*)
- Prof. Ph.D. Eng. Gilbert-Rainer Gillich, Department of Engineering Science, Babeș-Bolyai University, Cluj-Napoca, Romania, Faculty of Engineering, Piața Traian Vuia, nr. 1-4, 320085, Reşiţa, Romania gilbert.gillich@ubbcluj.ro
- Lect. Ph.D. Vasile-Catalin Rusu, Doctoral School of Engineering, Babes-Bolyai University, Cluj-Napoca, Romania, Faculty of Engineering, Piața Traian Vuia, nr. 1-4, 320085, Reşiţa, Romania vasile.rusu@ubbcluj.ro

Performance analysis of fluorescent and LED lighting sources

Elisabeta Spunei, Sorin Florin Dumitru, Cristian Paul Chioncel*, Florina Piroi

Abstract. *Artificial lighting is a necessity in the conduct of activities, especially at night. The use of fluorescent and LED lighting sources has led to a decrease in electricity consumption compared to incandescent lighting sources. The paper presents a case study highlighting the voltage and current waveforms in the operation of the analyzed sources. A considerable distortion of the current waveform is found, identifying the need for measures to improve power quality. The photometric measurements showed that for some light sources the luminous flux on the box is higher than the luminous flux actually emitted.*

Keywords: *lighting sources, electrical and photometric measurements, waveforms, efficiency*

1. Introduction

Electricity consumption by residential consumers is significant, accounting for around 30% of total European electricity consumption in 2017. Of this consumption about 15-20% was driven by the use of lighting installations [1]. Hence the need for a correct choice of lighting source.

In a 2013 study, the aim was to identify the type of lighting source that is most efficient. Efficiency was defined by considering average illuminance, maintenance cost, lifetime of sources and related equipment, power input, price and cost of energy consumed. The following types of lighting sources were analyzed: incandescent lamps, halogen lamps, compact fluorescent lamps, linear fluorescent lamps, and LED lamps. The analysis found that tubular fluorescent lamps are the most economical light sources [2].

In the case of fluorescent light sources, for faster priming, the auxiliary elements have been replaced by a high-voltage DC source, which is controlled by the pulse from a triac circuit. With this optimization, the service life was increased, the production cost was reduced, and the power consumption was reduced, since the priming coil was eliminated [3].

Since fluorescent lighting sources operate with a lower power factor than limit, it has been proposed to replace the classical ballast with an amplifier with two current sources: one using the supply voltage and another using a massive, charged capacitor from the amplifier's resonant circuit. This solution was tested on a 32W lamp [4].

In order to reduce electricity consumption in households, incandescent lighting sources have been replaced by LED (Light Emitting Diode) sources in recent years. In the United Kingdom, in 2007, it was found that this replacement led to a reduction in household electricity consumption of about 50.9% [5]. Another study [6] found that replacing halogen lighting sources in aircraft signage with LED sources led to a reduction in energy consumption of more than 57.3% and that the purchase and installation costs were 58% of the purchase and installation costs of halogen sources. This results in considerable savings that can be achieved.

Another method used to reduce energy consumption can be applied to new buildings. Thus in 2005 it was established that it is beneficial to use a window-to-wall ratio of about 0.20 [7]. This suggests the need for the wider use of daylighting and the choice of energy-efficient lighting sources.

The correct choice of the type of lighting source can only be made after proper design. This should consider the location of the lighting sources and the photometric curve so that the quality indicators of the lighting system are met [8, 9].

In all cases, a techno-economic analysis must be carried out to identify the cost, determine the payback time of the investment, the impact of the sources on the quality of the electricity [10, 11].

The paper presents a case study on one tubular fluorescent source, 5 fluorescent sources and 5 LED sources, both bulb types. Photometric measurements were also performed on toroidal fluorescent sources. Measurements were made on the electricity consumption, the luminous flux emitted, and their efficacy was calculated. The values from the measurements were compared with those on the nominal data box. To identify the impact of these sources on power quality, the waveforms of the supply voltage and the absorbed current were recorded. The analysis showed that there are cases where the data on the lighting source box do not correspond to the measurements, being lower. At the same time, a considerable distortion of the current waveform was found for LED and fluorescent sources.

2. Equipment used for measurements

To measure the luminous flux emitted by the analyzed sources, the Ulbricht lumenmeter (Fig. 1.a) was used in combination with the Unitest luxmeter (Fig. 1.b) mounted on the photometer.

Figure 1. Apparatus used to measure luminous flux: a) lumenmeter; b) luxmeter.

The measurement of electrical quantities (voltage, current, power, power factor, etc.) was carried out using the Chauvin Arnoux C.A. 8336 network analyzer (Fig. 2).

Figure 2. Network analyzer.

The lighting sources were placed on a specially designed and built teaching stand [12] (Fig. 3).

The stand has been designed in such a way as to allow the powering of a tubular LED bulb, 1, 2, 4 or 5 fluorescent or LED bulbs, as well as the simultaneous powering of all lighting sources.

The relation [12, 13-15] was used to determine the luminous flux Φ:

$$\Phi = \frac{E}{k} \ [\text{lm}] \tag{1}$$

where E is the illuminance measured with the luxmeter and k is the integrating photometer constant (k = 1.44), determined using a standard source.
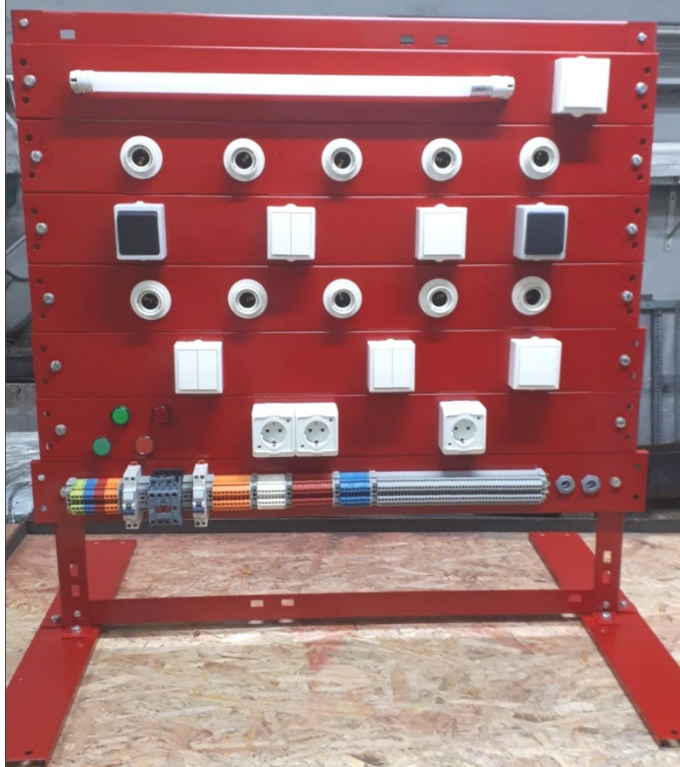

Figure 3. The used stand to study the operation of lighting sources.

The efficiency of the lighting source was calculated with the relation:

$$\text{e} = \frac{\Phi_n}{P_n} \left[\frac{\text{lm}}{W} \right] \tag{2}$$

where Φ_n is the nominal flux and P_n is the nominal wattage, both of which are commercial data marked on the lighting source box.

For comparison with measured or calculated sizes, the nominal sizes of the lighting sources were identified from their commercial box.

3. Measurements made

Table 1 shows the values identified from the lighting source box as well as the calculated magnitudes for the analyzed lighting sources [12].

Table 1. Electrical and photometric measurements identified, measured, and calculated.

Source type	Luminous flux [lm]		Rated power P_n [W]	Measured illuminance E [lx]	Nominal luminous efficacy e_n [lm/W]
	nominal Φ_n	calculated Φ_c			
Tubular LED	1100	1075	9	1548	122.22
LED bulb	1521	1534	17	2210	89.47
Fluorescent bulb	1450	1062.5	23	1530	63.04
Fluorescent toroidal	1200	881.9	20	1270	60.04

To measure power, current and power factor we used the network analyzer, which we set up accordingly. We measured the tube-type LED source, the 5 bulb-type LED bulbs connected in parallel, and the 5 bulb-types fluorescent bulbs connected in parallel. We did not take measurements for each bulb because the current value was too low and sometimes could not be measured with the network analyzer.

In order to get a picture of the waveforms we made recordings when the stand was powered, but without the lighting sources connected. The waveforms [12] of voltage (red color) and current (black color) are shown in Fig. 4.

2.1. Electrical measurements on tubular LED source

For the analysis of the operation of the tube-type LED source, it was powered via an autotransformer. The voltage at which the light source, with a low luminous flux, started to operate was 85 V, so much lower than the nominal supply voltage.

When connecting the tubular bulb, the maximum current value was 0.2 A and its waveform was strongly distorted by the electronic part in the tube (Fig. 5).
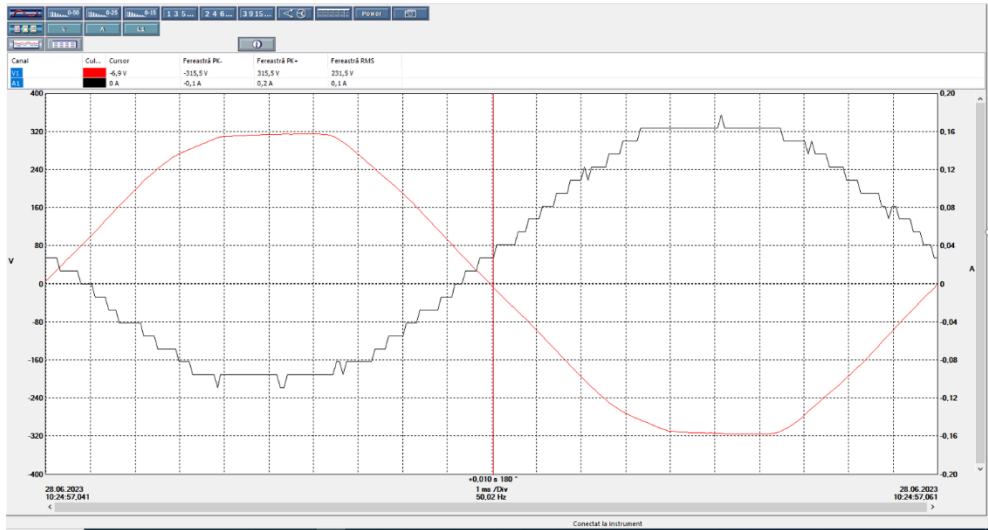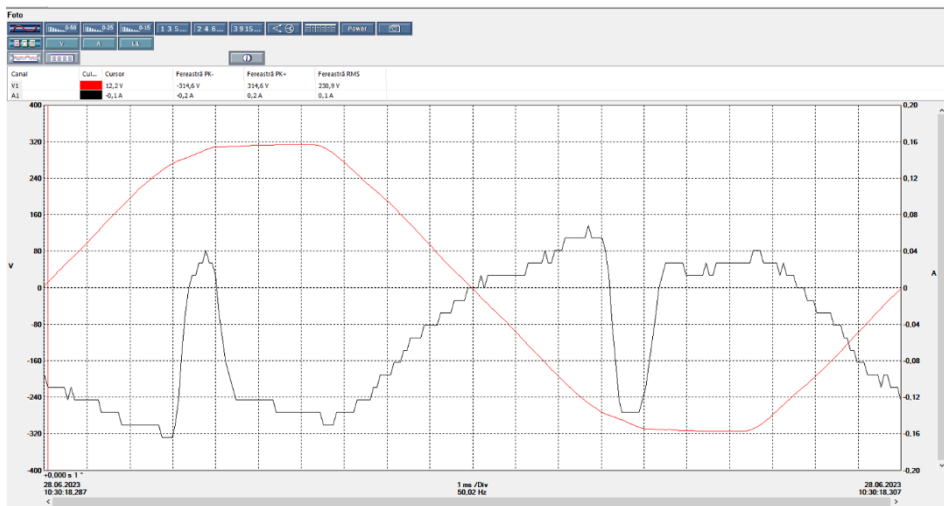
Figure 4. Voltage and current waveforms at stand power.

Figure 5. Voltage and current waveforms of the tubular LED source operation.

2.2. Electrical measurements on LED bulb sources

For this type of light source, the minimum voltage at which they started to emit luminous flux was 163.4 V, but with a very low luminous flux.

Since the current through a single LED bulb could not be recorded by the network analyzer, we connected 2 bulbs in series via ladder head switches. The voltage and current variation mode is shown in Fig. 6.

Figure 6. Voltage and current waveforms when operating 2 bulb-type LED sources.

There is a stronger distortion of the current waveform, and the maximum effective current value is 0.4 A.

In Table 2 we have presented the values of active power P, reactive power Q, apparent power S*, deforming power D, power factor cos φ and PF (power factor) [16]. In the table the power S* also takes into account the deforming power and PF takes into account the value of the angle λ between the active power P and the apparent power S*in the power-lipped.

Table 2. Values of powers and power factor corresponding to the operation of different types of sources in different assemblies

Mounting type	I_{max} [A]	P [W]	Q [VAr]	S* [VA]	D [VAr]	cos φ	PF
2 LED bulb	0.4	9.004	0.961	25.05	23.35	0.956	0.36
3 LED bulb	0.5	14.5	2.019	29.91	26.08	0.98	0.485
5 LED bulb	1	39.64	10.59	69.53	56.13	0.965	0.57
1 toroidal fluorescent	0.5	20.1	6.53	36.97	30.33	0.947	0.544

Mounting type	I_{max} [A]	P [W]	Q [VAr]	S* [VA]	D [VAr]	cos φ	PF
2 toroidal fluorescent	0.9	42.49	16.34	70.85	54.3	0.932	0.6
3 toroidal fluorescent	1.3	62.67	25.29	102	76.36	0.926	0.615
5 toroidal fluorescent	2	100.1	40.83	159.2	116.8	0.925	0.629
1 tubular LED, 5 LED bulb, 5 toroidal fluorescent	2.5	135	51.18	205.9	146.8	0.935	0.656

2.3. Electrical measurements on toroidal fluorescent toroidal lighting sources

In this type of sources, we have identified the priming voltage by using the autotransformer. We found that they prime at 132 V and light up to 43.2 V. And for this type of lighting sources, we made measurements with one toroidal fluorescent connected, with two, with three and with 5 toroidal fluorescent. In Fig. 7 we have shown the waveforms for a single connected toroidal fluorescent lighting sources and in Fig. 8 we present the waveforms with 5 toroidal fluorescent lighting sources.

It was found that the maximum value of the current was 0.5 A. The values of the powers and power factor for different power supply configurations are shown in Table 2.

2.4. Electrical measurements on power supply to all lighting sources on the stand

In Fig. 9 we have shown the voltage and current waveforms when all bulbs are connected (one tubular LED bulb, 5 LED bulbs and 5 toroidal fluorescent bulbs). The influence of the 5 fluorescent sources on the current waveform can be observed.

For this combination the maximum current value was 2.5 A. The values of power, power factor and PF are shown in Table 2.

Figure 7. Voltage and current waveforms in operation of a toroidal fluorescent lighting source.

Figure 8. Voltage and current waveforms during operation of 5 toroidal fluorescent lighting sources.

Figure 9. Voltage and current waveforms when operating with all bulbs on the stand.

4. Conclusion

Comparing the luminous flux values written on the light source boxes with the measured flux values shows that the luminous flux values of the LED tube source and the fluorescent sources are lower than the values written on the box with the nominal bulb data.

The calculation of luminous efficacy shows that the highest efficacy is achieved by the tubular LED source, followed by the bulb type LED source and then the fluorescent ones.

The tube-type LED source is operated at 36.96% of rated voltage. So, such sources are not sensitive to voltage variations. There is a strong distortion of the current waveform through the tubular LED source.

In the case of the bulb type LED source, the voltage at which it came on was 71.04% of the nominal voltage, so much higher than in the case of the tube type LED source.

In the case of fluorescent lighting sources, it was found that a time of more than 10 minutes was required for their complete priming and the emission of a constant luminous flux. They start emitting luminous flux at a voltage of 132 V (56.9% of nominal voltage) and remain on until about 18% of nominal voltage.

The analysis shows considerable distortion of the current waveform. This means that solutions need to be found to improve power quality.

References

1   Palacios-Garcia E.J., Chen A., Moreno-Munoz A., Research note: Calculating spectral irradiance indoors, *Lighting Research & Technology*, 49(1), 2017, pp. 122-127.
2   Yi C.-W., Hur S.-K., The Comparison of Economical Efficiency of Indoor Light Sources, *Journal of the Korean Institute of Illuminating and Electrical Installation Engineers*, 32(9), 2018, pp. 1-4.
3   Rana M., Kabir A., Khan A.G., Design and fabrication of compact fluorescent lamp igniter using TRIAC-assisted high-voltage DC source, *Electronics Letters*, 52(4), 2016, pp. 308-310.
4   Ponce M., Arau J., Alonso J.M., Evaluation of the class E amplifier with two current sources used as a high-power-factor electronic ballast for compact fluorescent lamps, *Journal of Circuits Systems and Computers*, 13(3), 2004, pp. 631-649.
5   Wall R., Crosbie T., Potential for reducing electricity demand for lighting in households: An exploratory socio-technical study, *Energy Policy*, 37(3), 2009, pp. 1021-1031.
6   Heung S. J., The Consideration of the Development Testing for LED type In-pavement Aeronautical Lights, *The transactions of the Korean Institute of Electrical Engineers*, 61(3), 2012, pp. 140-148.
7   El Mohimen M.A., Hanna G., Krarti M., Analysis of daylighting benefits for office buildings in Egypt, *Journal of Solar Energy Engineering-Transactions of the ASME*, 127(3), 2005, pp. 366-370.
8   Spunei E., Piroi I., Piroi F., Optimizing Street Lighting Systems Design, *Analele Universităţii „Eftimie Murgu" Reşiţa, Fascicola de Inginerie*, 21(3), 2014, pp. 257-268.
9   Spunei E., Piroi I., Chioncel C.P., *The experimental determination of the luminous flux emitted by a few types of lighting sources*, International Conference on Applied Sciences (ICAS 2016), 25–27 May 2016, Hunedoara, Romania.
10   Spunei E., Frumuşanu N.M., Măran G., Martin M., Technical-Economic Analysis of the Solutions for the Modernization of Lighting Systems, *Sustainability*, 14, 2022, 5252.

11 Majithia C.A., Desai A.V., Panchal A.K., Harmonic analysis of some light sources used for domestic lighting, *Lighting Research & Technology*, 43(3), 2011, pp. 371-380.

12 Dumitru S.F., *Stand pentru studiul surselor de iluminat de tip LED şi fluorescente toroidale,* Proiect de diplomă, Universitatea Babeș-Bolyai, Facultatea de Inginerie, 2023.

13 Piroi I., *Instalații electrice și de iluminat*, Editura Eftimie Murgu, Reșița, 2009.

14 Mogoreanu N., *Iluminatul electric*, Editura Lumina, Chișinău, 2013.

15 Bianchi G., Mira N., Moroldo D., Gheorghescu A., Moroldo H., *Sisteme de iluminat interior şi exterior*, Ediția a-III-a revizuită, Editura Matrix Rom, București, 2001.

16 Spunei E., Piroi I., Piroi F., Matasaru G.Ș. *Impact of Electrical Equipment on the Power Factor*, International Conference on Applied Sciences ICAS 2023, 24-27 May 2023, Hunedoara, Romania.

Addresses:

- Lect. Dr. Eng. Elisabeta Spunei, Department of Engineering Science, Faculty of Engineering, Babeș-Bolyai University Cluj-Napoca, Romania, Faculty of Engineering, Piaţa Traian Vuia, nr. 1-4, 320085, Reşiţa, Romania
  elisabeta.spunei@ubbcluj.ro
- Eng. Sorin Florin Dumitru, Department of Engineering Science, Faculty of Engineering, Babeș-Bolyai University Cluj-Napoca, Romania, Faculty of Engineering, Piaţa Traian Vuia, nr. 1-4, 320085, Reşiţa, Romania
  dumitru.sorin@stud.ubbcluj.ro
- Assoc. Prof. Dr. Eng. Cristian-Paul Chioncel, Department of Engineering Science, Faculty of Engineering, Babeș-Bolyai University Cluj-Napoca, Romania, Faculty of Engineering, Piaţa Traian Vuia, nr. 1-4, 320085, Reşiţa, Romania
  cristian.chioncel@ubbcluj.ro
  ([*]*corresponding author*)
- Dr. Tech. Florina Piroi, Technical University Wien, ZFDM and Faculty of Informatics, Karlsplatz 13, 1040, Viena, Austria
  piroi@ifs.tuwien.ac.at

High-power system for acoustic excitation of plates

Rusalin Lucian Paun, Gilbert-Rainer Gillich*, Marius Condratiuc

Abstract. *This paper introduces a device dedicated to acoustic excitation for modal analysis of plates. A particular setup is requested since the system should produce acoustic excitation with high power in the 10…120 Hz frequency range. The system comprises a signal generator, an amplifier powered by a car starter or a battery, and a subwoofer. This system permits setting the generated frequency around the resonance frequency with reasonable frequency and amplitude stability. We present the system's design and test its performance on a rectangular plate. In our laboratory experiments, we achieved the desired structural behavior.*

Keywords*: modal analysis, acoustic excitation, subwoofer, frequency estimation.*

1. Introduction

Metallic and non-metallic structures can suffer damage or deviations from the constructive parameters for various reasons. These can be local or spread along the structure [1]. To find the damage parameters, we need to know the measured values of the resonance frequencies for different modes of the component elements of these: beams, plates, etc. Since the 1990s, various vibration-based defect detection methods have been described in detail in the literature [2]-[4]. Since defects produce a relatively small change in the modal parameters, a very accurate estimate of the changes is essential [5].

Structural excitation for modal analysis can be done by the environment in which the structure operates [6], or controlled excitation can be applied by an operator through a suitable system [7]. Different methods of applying controlled excitation are mentioned in the specialized literature: acoustic waves, piezoelectric elements, magnetic coils, or shakers.

The devices that produce these controlled excitations have different powers, depending on the field and place of use, the type of defect sought, and other limitations.

We propose a subwoofer for excitation, whose large surface area is proper to generate controlled excitation of metallic and non-metallic plates. The subwoofer has a high power (up to 300 W true RMS). It permits inducing mechanical oscillations with controlled frequency and amplitude to obtain different vibration modes of the different types of structures.

2. Design of the actuation system

Generally, modal analysis equipment consists of the excitation and the signal acquisition and processing system. This paper presents an acoustic excitation system, with the configuration illustrated in the block diagram's upper part (Figure 1). The excitation system's requirements include adjustable frequency, controlled time length, and precise positioning.
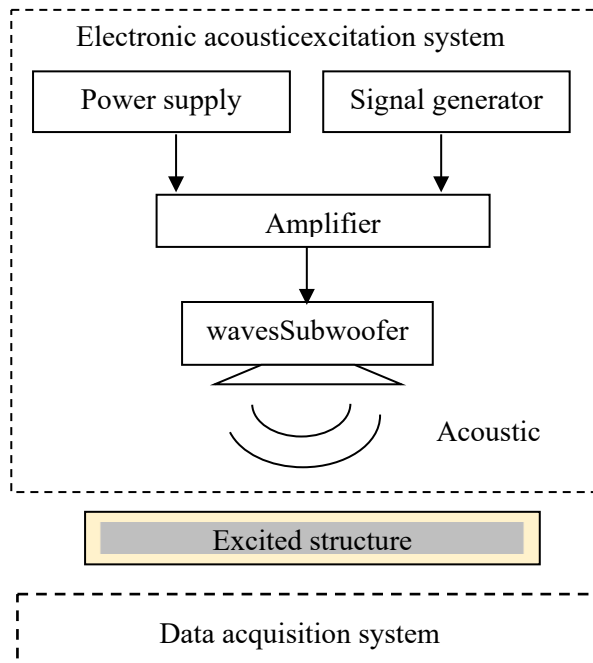
Figure 1. Actuation /acquisition system's functional block diagram

The excitation system should be able to generate frequencies in the range of 10-100 Hz. The acquisition system, which is not the aim of this paper but is used to prove the effectiveness of the excitation subsystem, can acquire accelerations up to 100 m/s^2 and accurately estimate the frequencies of short-time signals.

The developed acoustic excitation subsystem consists of a signal generator to produce a sinusoidal signal with adjustable amplitude and frequency, a subwoofer for audio bandwidth, an amplifier that drives the subwoofer, and connecting wires.

The used subwoofer is KIKER VCompS12, presented in Figure 2, and has the following characteristics:

   - 300 W Continuous Power (watt RMS) at 2 Ohm
   - 600 W Peak Power at 4 Ohm.

Since the sub-woofer's impedance is low, for practical reasons, we need a car amplifier powered at 12 Vdc.

Figure 2. Front and side view of the subwoofer KIKER VCompS12

The bandwidth of the subwoofer is from 25 to 120 Hz. If it is necessary to produce frequencies lower than 25 Hz, the frequency drop of the subwoofer can be compensated by increasing the gain using an ultra-low frequency amplifier.

One such amplifier is the BOSS Audio Systems MODEL R1600M. According to [18], it has the following parameters: Class A/B, Monoblock, MOSFET power supply; 1600 watts at 2-ohms x 1 max, 800 watts at 4-ohms x 1 max, High & low-level inputs; soft turn-on circuit, thermal overload speaker and short-circuit protection; Power &protect LEDs, variable low pass crossover 50–250 Hz; Variable bass boost 0–12 dB, variable gain control, speaker impedance 2–8 ohms; THD at RMS output: <0.01%, S/N ratio 102 dB, frequency response 9 Hz–130 Hz.

As the subwoofer has high power and frequencies around 50Hz are also generated, problems with grid network power noise can occur. Two usual solutions for powering the amplifier (each with advantages and disadvantages) can be used: batteries or a power rectifier.

Batteries are the best sources of direct current electricity supply. Unfortunately, they are heavy and cannot withstand a wide range of ambient temperatures without affecting their performance, discharge over time, etc.

Power rectifiers are more practical and can be moved more quickly. As a disadvantage, we mention that the power rectifiers can introduce noises with frequency multiples of the power grid frequency (especially at high powers and if they are not well matched to the amplifier) and are dependent on the presence of the power grid supply voltage. This last aspect can be eliminated today with portable electricity generators.

Fortunately, analyzing structural defects does not imply continuous use of the system but an intermittent use of relatively short duration. This particularity benefits both power supply methods: the batteries do not discharge during measurements, and a car starter can be used as a power rectifier, successfully replacing a battery for a short time.

One such car starter is the ever Active CBC-40 V2 charger, presented in Figure 3, which has start aid and the following main characteristics:

- Electronically stabilized output voltage - automatic charging process;
- Adjustable charging current - from 5A to 40A, for 12V/24V batteries;
- Digital ammeter;
- Max. charging current: 60A;
- Max. current for starting aid function: 300A;

Figure 3. Overview of the car charger

The charging current is enough to supply a 300 W amplifier, which can drive the subwoofer to the maximum RMS continuous power.

Figure 4. Overview of the front panel of the signal generator

The signal generator we use is of type BK PRECISION 4053 B and can generate stable and precise sine, square, triangle, pulse, noise, DC, and arbitrary waveforms [8]. The primary output voltage can be varied from 0 to 10 Vpp into 50 ohms (up to 20 Vpp into open circuit), and the secondary output can be varied from 0 to 3Vpp into 50 ohms (up to 6Vpp into open circuit). The modes of the generated signals can be modulated, swept, or burst. Modulation can be amplitude and frequency modulation (AM/FM), double side-band amplitude modulation (DSB-AM), amplitude and frequency shift keying (ASK/FSK), phase modulation (PM), and pulse width modulation (PWM). It also has a built-in counter.

Frequency accuracy is +25ppm, the resolution is 1μHz, and the bandwidth is 1μHz to 10MHz.

Amplitude accuracy is $\pm (1\% + 1$ mVpp of setting value) for 2 mVpp – 10 Vpp into 50 Ω (4 mVpp – 20 Vpp into open circuit), ≤ 10 MHz amplitude and the normal output impedance is 50 Ω for both channels.

Sweep shape can be linear or logarithmic, up or down. Time sweep is from 1ms to 500s, triggered internally, externally, or manually for a sinusoidal, square, ramp, or arbitrary waveform.

In this experiment, we use a sinusoidal frequency close to a plate's first natural frequency. Hence, we obtain a resonant response of the structure.

3. Testing the excitation system on plates

The excitation system is tested on a steel plate with the dimensions $a = 950$ mm and $b = 400$ mm. The thickness of the plate, which is clamped on the contour by fixing it in a specially designed restraining system, is $t = 2$ mm. The first natural frequency is determined with the FEM in [9], and we found it is $f_1 = 73.047$ Hz.
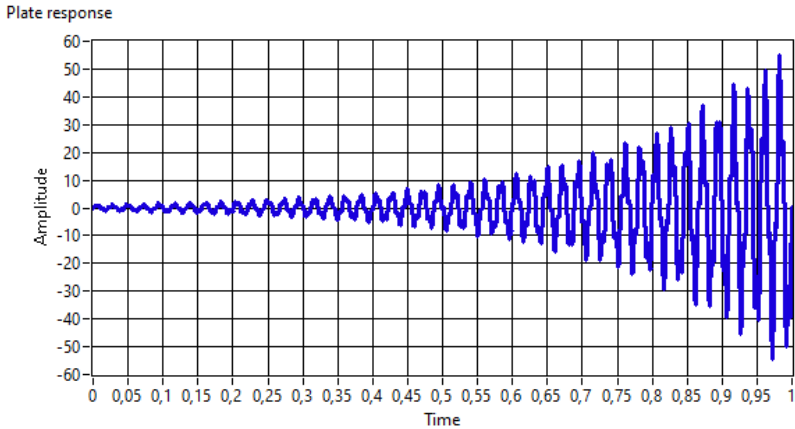

Figure 5. Response of the lightweight structure (plate clamped on the contour)

The signal obtained in the first second of excitation is presented in Figure 5. The acquisition system is comprehensively described in [10]. One can observe that the amplitude increases rapidly, and the alteration of the first mode is minimal.
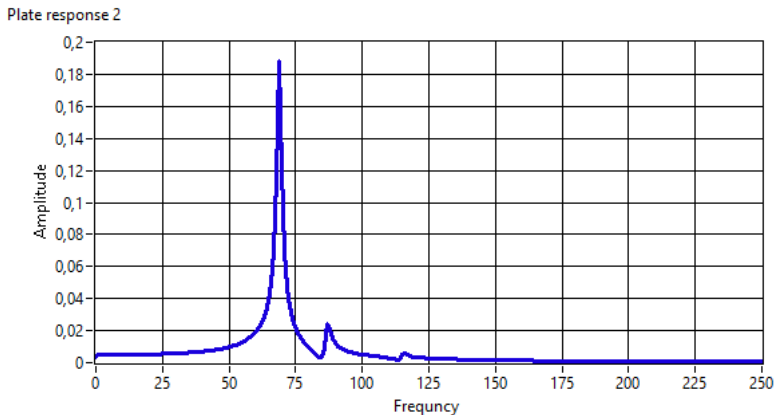
Figure 6. Response of the lightweight structure in the frequency domain

The relevant harmonic component at approximately 70 Hz can be observed in Fig. 6, which confirms the clear pseudo-sinusoidal evolution of the signal. Given the excellent quality of the response signal, which demonstrates that we control how the energy is transferred to the structure, we conclude that the designed system is proper for experimental modal analysis.

4. Conclusion

The paper presents a non-contact method to excite lightweight structures with acoustic pressure with controlled energy. The control concerns the frequency, thus the excited vibration mode, and the amplitude of this mode. We proved that when using a controlled excitation, the signal is close to a pseudo-sinusoidal signal, whose spectrum contains a strong harmonic component and several harmonics with low amplitude. This spectrum is proper for estimating the frequencies with high accuracy. The disadvantage is the one-by-one search of the harmonic components and their frequency. In the following studies, we will test the excitation system with a swept-sine signal to excite more vibration modes and get their frequencies.

References

1   Gillich G.R., Praisach Z.I., Iancu V., Furdui H., Negru I., Natural Frequency Changes due to Severe Corrosion in Metallic Structures, *Strojniški vestnik - Journal of Mechanical Engineering*, 61(12), 2015, pp. 721-730.
2   Doebling S., Farrar C., Prime M., A summary review of vibration-based damage identification methods, *Shock and Vibration Digest*, 30, 1998, pp. 91-105.
3   Gillich G.R., Tufoi M., Korka Z.I., Stanciu E., Petrica A., The Relations between Deflection, Stored Energy and Natural Frequencies, with Application in Damage Detection, *Romanian Journal of Acoustics and Vibration,* 13(2), 2016, pp. 87-93.
4   Salawu O., Detection of structural damage through changes in frequency: a review, *Engineering Structures*, 19(9), 1997, pp. 718–723.
5   Minda A.A., Barbinita C.I., Gillich G.R., A Review of Interpolation Methods Used for Frequency Estimation, *Romanian Journal of Acoustics and Vibration*, 17(1), 2020, pp. 21-26.
6   Hearn G., Testa R., Modal analysis for damage detection in structures, *Journal of Structural Engineering*, 117, 1991, pp. 3042-3062.
7   Zahid F.B., Ong Z.C. Khoo S.Y., A review of operational modal analysis techniques for in-service modal identification, *Journal of the Brazilian Society of Mechanical Sciences and Engineering*, 42, 2020, art. 398.

8   BK Precision website www.bkprecision.com (downloaded on October 12th, 2023)

9   Haţiegan L.B., Haţiegan C., Gillich G.R., Hamat C.O., Vasile O., Stroia M.D., Natural frequencies of thin rectangular plates clamped on contour using the Finite Element Method, *IOP Conference Series: Materials Science and Engineering*, 294(1), 2018, art. 012033.

10 Mituletu I.C., Gillich G.R., Maia N.M.M., A method for an accurate estimation of natural frequencies using swept-sine acoustic excitation, *Mechanical Systems and Signal Processing*, 116, 2019, pp. 693-709.

Addresses:

- Ph.D. Stud. Eng. Rusalin Lucian Paun, Doctoral School of Engineering, Babes-Bolyai University, Cluj-Napoca, Romania, Faculty of Engineering, Piaţa Traian Vuia, nr. 1-4, 320085, Reşiţa, Romania, rusalin.paun@ubbcluj.ro
- Prof. Ph.D. Eng. Gilbert-Rainer Gillich, Department of Engineering Science, Babeș-Bolyai University. Cluj-Napoca, Romania, Faculty of Engineering, Piaţa Traian Vuia, nr. 1-4, 320085, Reşiţa, Romania, gilbert.gillich@ubbcluj.ro
  ([*]*corresponding author*)
- Stud. Marius Condratiuc, Department of Engineering Science, Babeș-Bolyai University. Cluj-Napoca, Romania, Faculty of Engineering, Piaţa Traian Vuia, nr. 1-4, 320085, Reşiţa, Romania, marius.condratiuc@stud.ubbcluj.ro

Crimping Standard DIN vs USCAR Gap Analysis

Florin Dragomir, Tiberiu Manescu*, Zeno-Iosif Praisach

Abstract. *In this paper the main objective is to present the current status of the automotive specifications related to the crimping process, an in particular how these specifications were adopted by the suppliers of the crimping components (e.g. Terminals and cables). For this reason, we took as reference two of the most worldwide used standards form the automotive manufacturing industry: DIN ("Deutsches Institut für Normung") with the corresponding Romanian standard SR EN 60352-2:2006 and SAE/USCAR-21 REVISION 3.*

Keywords*: crimping standard, gap analysis, crimping microsection, statistical analysis, crimping compression*

1. Introduction

In the current world of automotive wiring harness manufacturing industry one of the critical processes is the crimping assembly between the wiring cable and the terminals design by the OEM's. Due to this reason all Original Equipment Manufactures in automotive industry were adopting a common approach to issue a set of specifications that will enable a higher stability and subsequently a higher quality of the product throughout product lifetime [1], [2].

As the biggest markets from the world European Union and US manufacturers were adopting specific norms to define and control the crimping process like DIN (SR EN 60352-2:2006) and SAE/USCAR-21 Rev 3.

The purpose of this paper is to evaluate how the crimping process specifications in both these standards fit together and where there are gaps, how these gaps influence the current production process of the component suppliers and, finally, to have a better understanding of potential optimization of the crimped assembly from a productivity, quality, and financial indicators point of view.

To enable us to do the analysis, we focus our research on the critical parameter requirement of a crimped splice assembly between a copper plated terminal and a standard FLRY-A wire with a cross section of 0.50 [3], [4].

Our objective was to analyze the compression specifications in both European and US standards and to construct a gap analyze of the main specification, and in the second stage of the study to observe the influence of these specification and how these standards were introduced in a operational environment. The paper is a starting point in the quest to determine using statistical analysis tools the optimum compression requirement that will enable wiring systems manufacturers to have a clear standard specification when validating the crimp-joint.

This will enable a significant improvement of the overall manufacturing cost incurred by the wear and tear of the active parts on any applicator tool due to the tendency of the tools manufacturing suppliers to increase the percentage of the compression factor which will secure a better resistivity but by doing this negatively influencing significantly the life time of the crimp applicator tool.

2. Methodology

The study was structured in two distinct steps that enable was to investigate the theoretical implication of the specification over the compression characteristics of a crimped assembly and how this specification was adopted in a real manufacturing environment.

In the first step we put together a Gap Analyze chart focused on the specification that control the behavior of the compression of a crimped assembly as specified in both standards (Table 1).

Table 1. Gap Analysis on compression specification

Specification details	SR EN 6032-2:2006	SAE/USCAR-21 Rev.3
Degree of compression	Not specified	From 15% to 20% upward as minimum requirement
Quality of the crimped microsection	Not specified	Quality of the crimped area influenced by the compression and controlled by the crimping tool and terminal design. It is recommended to document the cable cross section of the cable used in production to be in accordance with the one used for terminal validation
Compression specification limits	Not define LSL or USL	Not specified (LSL – just as indication start from 15%-20%) No Upper Limit

Specification details	SR EN 6032-2:2006	SAE/USCAR-21 Rev.3
Cycle Current Test		
Correlation between Compression/Pull test/Resistance	Not specified	

By analyzing the outcome of the gaps what we clearly observed is that the European Standard has a much general approach and is leaving a high degree of freedom to the components suppliers to define their own operational standards. By comparation the USCAR have a more specific requirements in relation to the compression and to the general aspect of the cross section but also the approach is very general and is allowing the suppliers to develop their own specifications.

As summary of the gap analysis, we observed that related to the compression and general requirements of a standard output in a crimped process we will need to achieve a minimum 15% to 20% compression rate without any specification on upper limit, the general aspect of the cross section needs to be defined and documented by the component manufacturer and that the test currents are significant different EN standard specifying half the values.

Having this as a base to further understand the impact inside a real production environment we selected as second step in our study a Schaefer eps 2000 (Fig. 1), and 75 crimping tools (Fig. 2). All the crimping tools were set to enable a crimped assembly between 75 terminals specific for 0.50 mm² cross section and a FLRY-A cable 0.50 mm² in cross section:
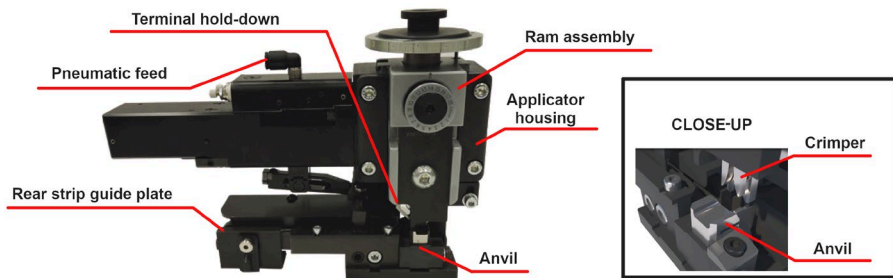
Figure 1. Schaefer eps 2000 crimping machine

Figure 2. Crip tooling: applicator parts and close-up of inserts

For all the 75 combinations between terminal and cable we used a set of 125 samples for which we performed microsection analysis using a test equipment Komax Microlab35 (Fig. 3) and pull test capability study.

Figure 3. Komax MICROLAB 35

All the datasets were collected in a Data Collection Plan to enable our team to perform with the help of Minitab software a more comprehensive analysis [5], for a better understanding of the compression behavior in a real production environment and by performing statistical analysis to determine a statistical relevance of that behavior. In addition, for each terminal-cable assembly we performed a capability study on pull test to understand the behavior of the CmK (Capability Index) across the full sample range.

3. Data analysis and assumptions

The Data Collection Plan presented in Table 2 was focused in collecting the type of the terminal used, the wire cable the compression obtained after the crimping process and the Capability index on the pull test performed.

Table 2. Data Collection Plan (extract)

Nr. Crt.	Applicator	Terminal part number	Supplier	Cross section cable	Cable Type	Comp-ression	CmK pull test
1	CV-001-B	P00005123	TYCO	0.50	FLRY-A	76.20%	3.96
2	CV-001-B	P00039988	TYCO	0.50	FLRY-A	75.12%	4.09
3	CV-003-N	P00009924	TYCO	0.50	FLRY-A	75.00%	3.72
4	CV-003-M	P00009926	TYCO	0.50	FLRY-A	79.00%	3.22
5	CV-005-L	P00106149	TYCO	0.50	FLRY-A	76.60%	3.64
6	CV-005-L	P00106155	TYCO	0.50	FLRY-A	76.60%	3.82
7	CV-006-B	P00005035	TYCO	0.50	FLRY-A	74.20%	2.5
8	CV-009-A	P00009916	TYCO	0.50	FLRY-A	81.20%	2.51
9	CV-012-B	P00005162	TYCO	0.50	FLRY-A	72.00%	4.84
10	CV-015-E	P00001731	TYCO	0.50	FLRY-A	76.60%	2.8
11	CV-015-E	P00004238	TYCO	0.50	FLRY-A	71.40%	4.32
12	CV-021-A	413003926	LEAR	0.50	FLRY-A	75.00%	4.92
13	CV-025-B	P00002984	TYCO	0.50	FLRY-A	78.60%	5.41
14	CV-033-I	P00005553	TYCO	0.50	FLRY-A	83.00%	2.49
15	CV-035-B	P00009976	TYCO	0.50	FLRY-A	74.20%	4.54
16	CV-052-A	P00002178	TYCO	0.50	FLRY-A	74.25%	2.49

Looking over the data collected from the beginning it was clearly visible that the range of the compression values was quite high and to have a statistical overview of the data we performed an I-MR Chart on compression (Fig.4) and for better understanding of the process stability we completed the data analysis with a Boxplot chart (Fig.5).
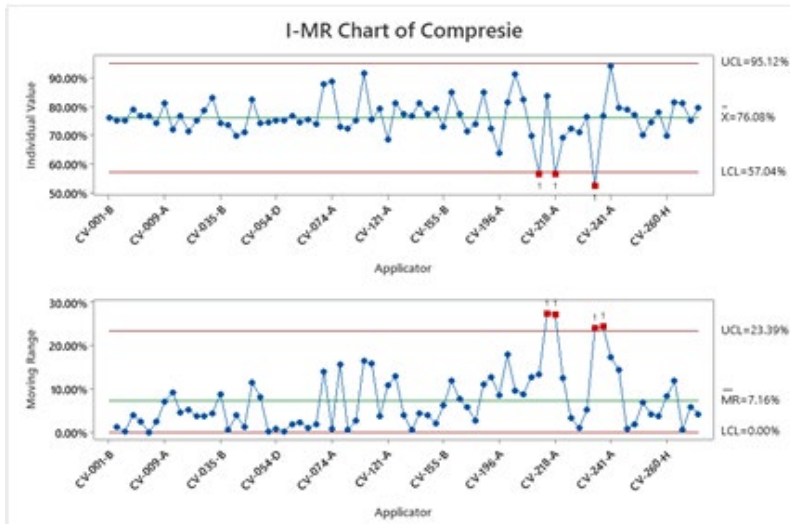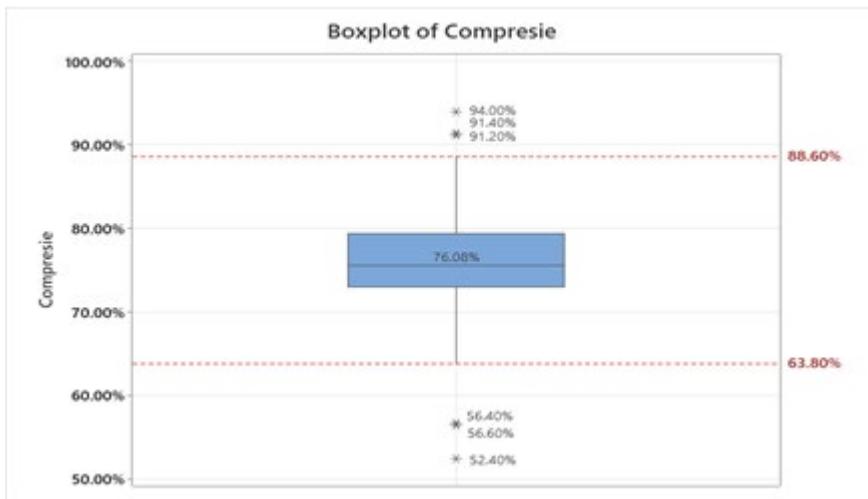
Figure 4. Control chart of Compression

Figure 5. Boxplot analysis of Compression

In both charts the data analyzed shows that the process is a stable one with a average around the compression value of 76% and in the Box plot chart we see that the minimum compression registered is 52.4% and the maximum is 94%. Also analyzing the evolution of the CmK index at the pull test it is clear that the pull test process is also very stable with high capability index.

52

4. Conclusions

After observing the range of all the compression level values and the minimum and maximum related to the pull test Capability Index, as well as the investigation carried out to understand the requirements of European and US standards we can conclude that it is necessary to introduce a predictive model, [6], which allows wiring systems suppliers to better understand the limits of the compression and basically to enable them to obtain an optimum ratio between compression percentage of a crimped cross section and pull test and subsequently the resistance of the specified crimped joint.

As showed in the current study each supplier can develop his own standards that due to the too general specifications of the European Standards and US standards will fit in within the general requirements and be treated on a case-by-case basis, without a real potential of predicting an optimal cluster of specifications [7].

The current study shows that the control limits of the compression for an optimal crimping process is inside 63.8% to 88.6% interval. If we want to translate this into lifetime cycle of an active part for a crimping applicator tool, we will observe that operating on the upper specification limit the operational lifespan of the tool will decrease with more than 50% which will have as immediate effect a 50% increase in the spare part consumption. This shows the need for a clear more strict specification on compression to enable tool manufactures and wiring harness supplier to align and to follow that optimum specification when validating a new crimp joint assembly.

References

1 SAE International, *Performance Specification for Cable-to-Terminal Electrical Crimps. SAE/USCAR-21*. 4th SAE International, U.S. and Canada, 2020.
   https://global.ihs.com/doc_detail.cfm?document_name=SAE%20USCAR%2D21&item_s_key=00407431

2 SR EN 6032-2:2006/A1:2014, Solderless connections, Part2: Solderless crimped connections, General Requirements, test methods and practical guidance.
   https://magazin.asro.ro/ro/standard/224996

3 Mocellin K., Petitprez M., Experimental and Numerical Analysis of Electrical Contact Crimping to Predict Mechanical Strength, *Procedia Engineering*, 81, 2014, https://doi.org/10.1016/j.proeng.2014.10.274

4   Morgado L., Teixeira A., Sá J., Pinto Ferreira L., Almeida F.D., Analysis and Development of a Failure Prediction Model for Electrical Terminals Used in the Automotive Industry, *Procedia Manufacturing,* 51, 2020, pp. 207-214, https://doi.org/10.1016/j.promfg.2020.10.030.

5   Delozier M.R., Orlich S., Discovering influential cases in linear regression with MINITAB: Peeking into multidimensions with a MINITAB macro, *Statistical Methodology*, 2(2), 2005, pp. 71-81, https://doi.org/10.1016/j.stamet.2004.11.005

6   Ilca D., Manescu T., Gillich G.-R, Praisach Z.-I., Tufisi C., Determination of proper parameters for ultrasonic welding of copper plate with copper wire strands, *Vibroengineering Procedia*, 51, 2023, 173-178, https://doi.org/10.21595/vp.2023.23680

7   Castro T.A.M., Campilho R., Optimising a Specific Tool for Electrical Terminals Crimping Process, *Procedia Manufacturing*, 11, 2017, pp.1438-1447, https://doi.org/10.1016/j.promfg.2017.07.274

Addresses:

- Ph.D. Stud. Eng. Florin Dragomir, Doctoral School of Engineering, Babeș-Bolyai University, Cluj-Napoca, Romania, Faculty of Engineering, Piața Traian Vuia, nr. 1-4, 320085, Reşiţa, Romania florin.dragomir@ubbcluj.com
- Assoc. Prof. PhD. Habil. Eng. Tiberiu Manescu, Doctoral School of Engineering, Babeș-Bolyai University, Cluj-Napoca, Romania, Department of Automation, Industrial Engineering, Textiles and Transportation, Aurel Vlaicu University, Bd. Revoluției 77, 310032, Arad, Romania manescu.tiberiu@gmail.com
  (*corresponding author*)
- Lect. Ph.D. Eng. Zeno-Iosif Praisach, Babeș-Bolyai University, Cluj-Napoca, Romania, Department of Engineering Science, Babeș-Bolyai University, Cluj-Napoca, Romania, Babeș-Bolyai University, Faculty of Engineering, Piața Traian Vuia, nr. 1-4, 320085, Reşiţa, Romania zeno.praisach@ubbcluj.ro

Crimping Tool Wear and Tear Analysis

Dacian Ilca, Tiberiu Manescu*, Cristian Tufisi

Abstract. *This paper represents an investigation into spare parts longevity in the context of automotive production. By systematically examining the accuracy of the crimping process, our research unveils the potential for cost reduction by pushing the limits of the usage of crimping tooling, while maintaining production efficiency and quality. Preliminary findings reveal encouraging prospects, but underscore the necessity for further examinations, maintenance strategies, and the development of predictive models. Through the tests described in this paper and the obtained results, it has been concluded that the limits imposed by the procedure can be extended (thus reducing production interruptions and associated costs). Extending these limits cannot be determined by a universally applicable rule, therefore, additional analyses are necessary, analyses that will be the subject of further research.*

Keywords*: crimping process, spare parts lifetime, anvil, crimper, value engineering*

1. Introduction

The automotive industry faces relentless competition, evolving market demands, and stringent regulations, which drive the constant quest to cut production costs while upholding product quality and performance. This drive has given rise to the practice of value engineering, focusing on enhancing product efficiency while minimizing expenses [1], [2].

Within this context, a critical factor to consider is the longevity of spare parts used in specialized machinery. These often-overlooked components wield significant influence over cost-efficiency and productivity within automotive plants.

This paper aims to evaluate cost reduction possibilities in an electrical harness production plant by investigating the lifespan of spare parts employed in the crimping process. The crimping process is fundamental to electrical and electronic assembly, vital for creating reliable wire-to-connector connections in various industries, including automotive manufacturing.

As the crimping tool's active parts endure wear and tear during regular use, they require replacement, impacting overall project costs. Standard maintenance protocols given by the crimping equipment suppliers typically recommend active part replacement when wear or damage is detected. Internally, work instructions dictate replacement after ½ years or at 200000 crimps (strokes). While efforts have been undertaken, there are presently no accurate methods for predicting the failure of spare parts [3], [4].

Our objective is to conduct tests to assess the validity of the 200000-stroke reference point for active part replacement and explore alternative methods for determining replacement, potentially extending the tooling's lifespan. We hypothesize that significant differences in spare parts wear exist among various crimping tools, which may necessitate a reconsideration of the current internal instructions.

This study aims to advance the current state of the field by introducing novel insights based on empirical analyses, thus opening up space for an integrated body of knowledge. By meticulously examining the accuracy of the crimping process in automotive production, our research not only extends the established boundaries but also suggest cost-effective methodologies to minimize production interruptions and expenses. This work's paramount contribution lies in its revelation of unexplored opportunities for enhancing longevity in spare parts, thereby fortifying the foundation for more efficient and economical manufacturing practices. The imperative necessity to optimize maintenance strategies and develop predictive models is underscored, highlighting the indispensable relevance of this research in steering the industry towards more robust and forward-thinking methodologies.

2. Methodology

The machine used for this study is a Schaefer eps 2000 (Fig. 1), used alternatively with two different crimping tools (applicators) from TE. The two critical tooling inserts within an applicator are the wire crimper and the anvil, commonly known as the active parts or spare parts (Fig.2).

The wear of the applicator active parts can be determined indirectly by examining the results of a crimp. In the context of this investigation, we have evaluated two distinct applicator types belonging to the same family (designated App_01 and App_02). We have used a cable with cross section 0.35mm2 type FLRY-A and two terminals with the same material (CuNiSi).

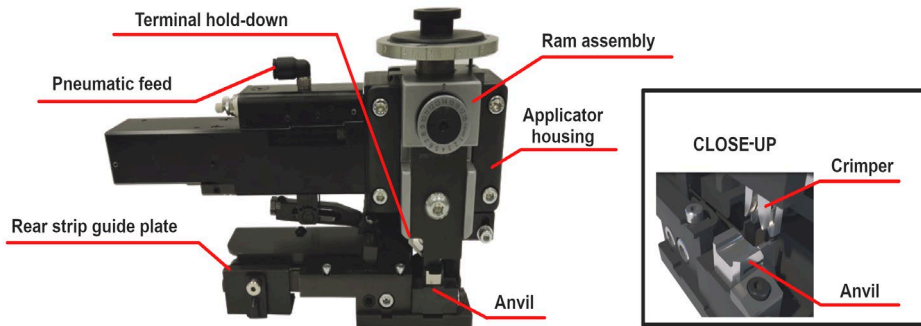**Figure 1.** Schaefer eps 2000 crimping machine

Figure 2. Crip tooling: applicator parts and close-up of inserts

Our initial step involved recording the baseline value, as documented by the strokes-meter of each applicator. Given the extended duration of the testing, we introduced a protocol for measurement intervals, set at either every 5 working days or when the cumulative strokes reached 60000, depending on whichever milestone occurred first. At each of these designated points in time, we conducted assessments and measurements of the quality of the crimps, recording the results in a table. If the measured parameters were off scale, the experiment stopped and the final value on the meter was recorded. If no deviation was found after twenty iterations of testing, provided that the limit of 200000-strokes has been exceeded, the experiment was also stopped and the value on the meter recorded.

Evaluating the crimp quality is a method commonly used in the industry [5]-[7] and consists of specific steps and measurements, such as visual inspection: correct crimp (Fig. 3) or incorrect crimp (Fig. 4), cross section analysis (Fig. 5) and others.

In essence, a quality crimp ensures that the wire maintains the right shape and size without any excess material, deformities, or damage that might lead to connection failures [8].
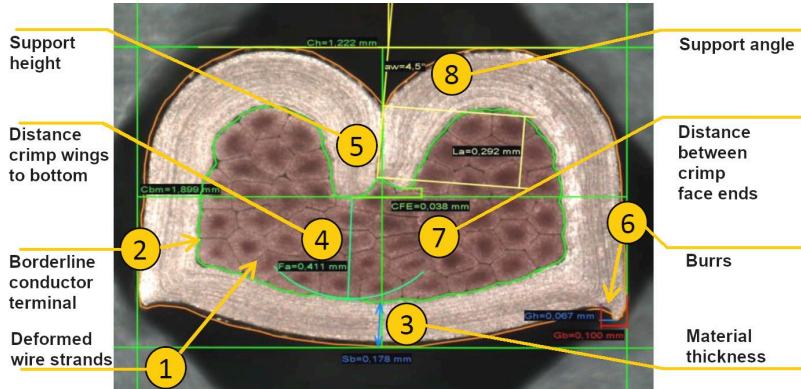

Figure 3. Microsection of the crimp, showing measurable parameters
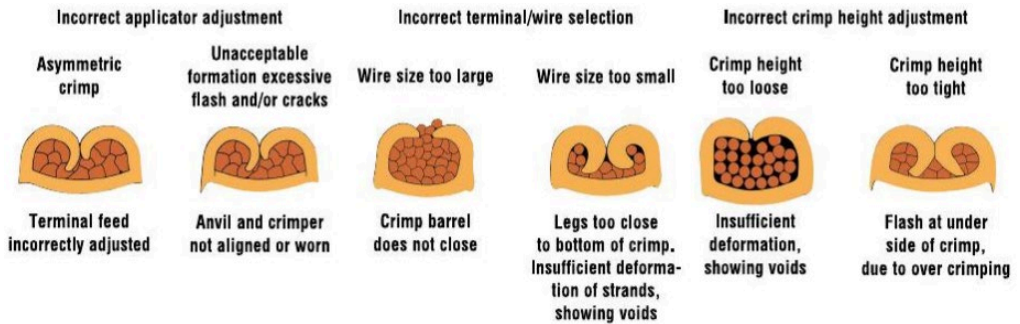

Figure 4. Incorrect crimp quality

A high-quality crimp should achieve the necessary area reduction without causing issues like flash (burr), over-crimping, under-crimping, or bending, respecting the nominal intervals for given value measurements (Fig. 5).

We applied the previously outlined methods to evaluate the crimp's quality and generated a dataset of values that were analyzed in Minitab software. The most significant parameters in our study are wire crimp height (CH), wire crimp width (CW), burr height (Gh) and burr width (Gb). Especially the latest two are indicative of spare parts wear or damage.
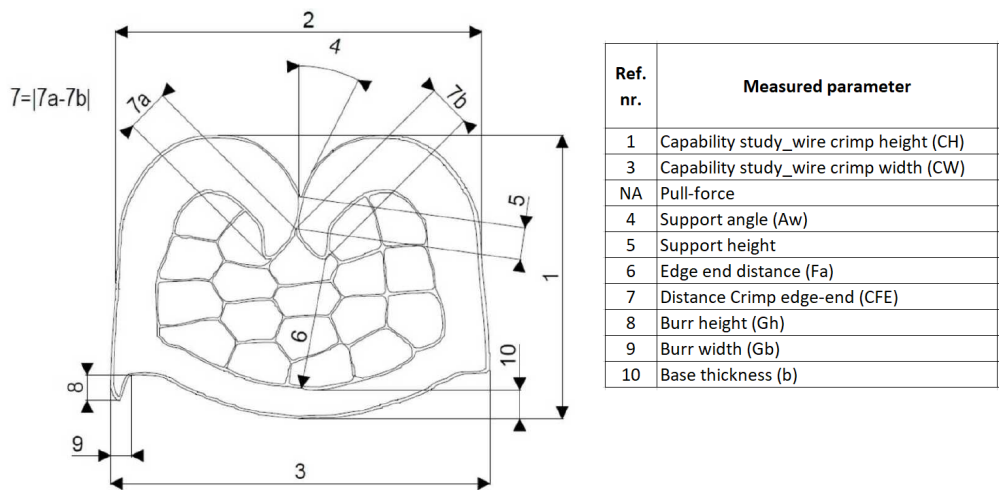
Ref. nr.	Measured parameter
1	Capability study_wire crimp height (CH)
3	Capability study_wire crimp width (CW)
NA	Pull-force
4	Support angle (Aw)
5	Support height
6	Edge end distance (Fa)
7	Distance Crimp edge-end (CFE)
8	Burr height (Gh)
9	Burr width (Gb)
10	Base thickness (b)

Figure 5. Crimp cross section measurable parameters

3. Data analysis and discussion

The dataset presented in Table 1 was collected through a series of test iterations focusing on the resulted crimps of two applicators, App_01 and App_02, with the aim of drawing insights and conclusions about their active parts wear and tear.

In line with our study's design, we concluded the experiment for App_01 after twenty recorded instances, even though the achieved crimps remained within the specified range (Fig. 6, 7). The initial meter reading of App_01 was 9308462, and the final reading reached 10163418, resulting in a cumulative total of 854956 strokes performed for quality crimps.

Table 1. App_01 Tests iterations and measured values of parameters

Nr. Crt.	Strokes number	Capability study wire crimp height CH 0.76 ±0.03 mm	Capability study wire crimp width CW 1.40+0.15 mm	Burr height Gh ≤0.20 mm	Burr width Gb ≤0.10 mm
1	9308462	0.7580	1.4070	0.0000	0.0000
2	9336012	0.7730	1.4210	0.0000	0.0000
3	9362092	0.7630	1.4640	0.0000	0.0000
4	9381825	0.7770	1.4540	0.0000	0.0000
5	9404857	0.7770	1.4510	0.0000	0.0000
6	9441572	0.7730	1.4450	0.0540	0.0000

Nr. Crt.	Strokes number	Capability study wire crimp height CH 0.76 ±0.03 mm	Capability study wire crimp width CW 1.40+0.15 mm	Burr height Gh ≤0.20 mm	Burr width Gb ≤0.10 mm
7	9479197	0.7810	1.4500	0.0000	0.0000
8	9519222	0.7550	1.4280	0.0400	0.0770
9	9544204	0.7670	1.4360	0.0500	0.0500
10	9569809	0.7730	1.4440	0.0000	0.0000
11	9630170	0.7740	1.4420	0.0000	0.0000
12	9690192	0.7560	1.4230	0.0260	0.0880
13	9750445	0.7780	1.4280	0.0000	0.0000
14	9777968	0.7650	1.4250	0.0000	0.0000
15	9822351	0.7730	1.4440	0.0000	0.0000
16	9882407	0.7640	1.4620	0.0000	0.0000
17	9931873	0.7600	1.4320	0.0330	0.0980
18	9956797	0.7790	1.4380	0.0000	0.0000
19	10051447	0.7840	1.4410	0.0800	0.0330
20	10163418	0.7860	1.4390	0.0210	0.0880

Remarkably, the cumulative number of strokes, which reached 854956, greatly exceeded the reference point of 200000 strokes as per the recommended spare parts exchange. This significant surplus in the number of strokes observed suggests a potential for extending the operational lifespan of the equipment.
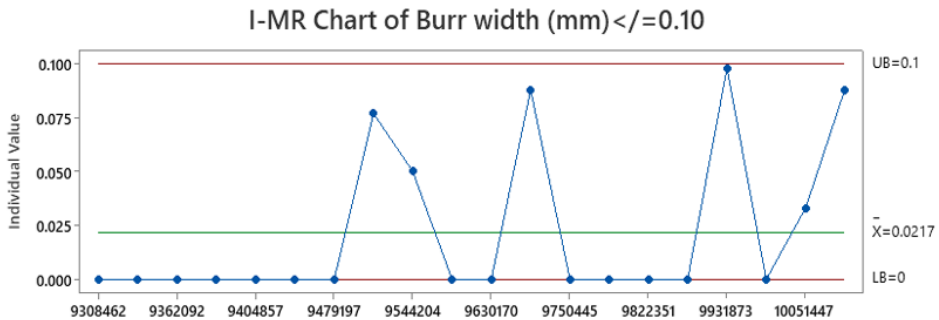

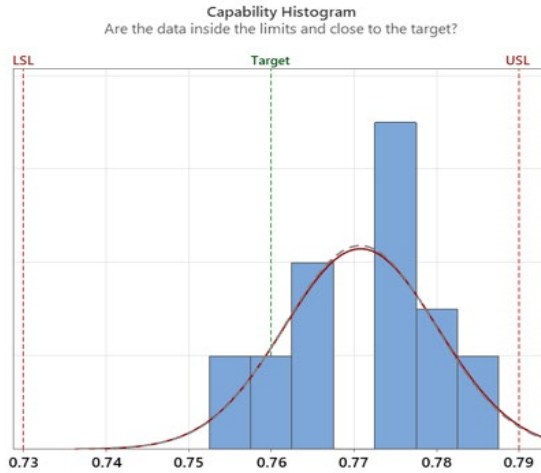**Figure 6.** Control chart of the burr width for App_01

Figure 7. Histogram analysis of crimp height for App_01

Concerning App_02, the experiment was concluded after sixteen iterations (see Table 2) due to an observed defect.

Table 2. App_02 Tests iterations and measured values of parameters

Nr. Crt.	Strokes number	Capability study wire crimp height CH 0.78 ±0.02 mm	Capability study wire crimp width CW 1.07+0.11 mm	Burr height Gh ≤0.20 mm	Burr width Gb ≤0.10 mm
1	2299978	0.7800	1.0990	0.0000	0.0000
2	2312128	0.7970	1.1400	0.0000	0.0000
3	2325693	0.7750	1.1620	0.0000	0.0000
4	2336993	0.7650	1.1350	0.0000	0.0000
5	2358030	0.7730	1.1510	0.0000	0.0000
6	2380845	0.7850	1.1490	0.0000	0.0000
7	2397279	0.7970	1.1630	0.0000	0.0000
8	2406379	0.7880	1.1520	0.0340	0.0520
9	2429907	0.7970	1.1400	0.0000	0.0000
10	2447082	0.7730	1.1510	0.0000	0.0000
11	2471040	0.7650	1.1400	0.0000	0.0000
12	2485118	0.7970	1.1630	0.0000	0.0000
13	2491843	0.7710	1.1380	0.0210	0.0370
14	2505343	0.7840	1.1620	0.0000	0.0000
15	2522143	0.7980	1.1750	0.0000	0.0000
16	2553490	0.7860	1.1480	0.0640	0.1050

The deviation from the anticipated values was identified through the measurement of the burr width (Fig. 8). While the measurements for crimp height and width remained within acceptable ranges (Fig. 9), the observed deviation in burr width suggests a potential concern regarding the wear and tear of the anvil (as depicted in Fig. 10).
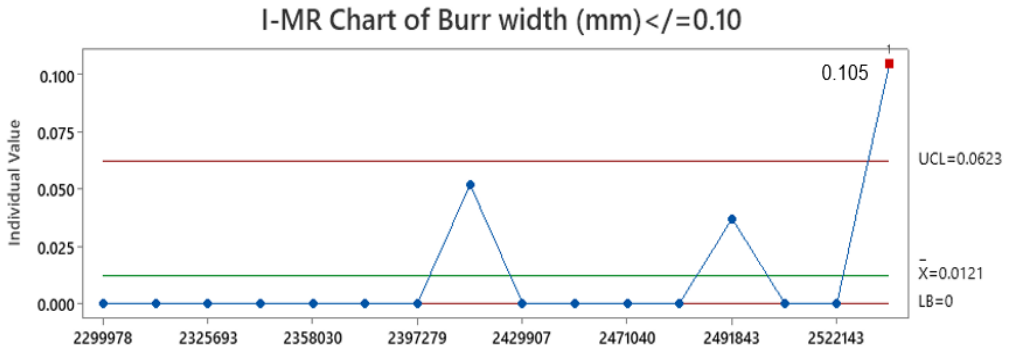

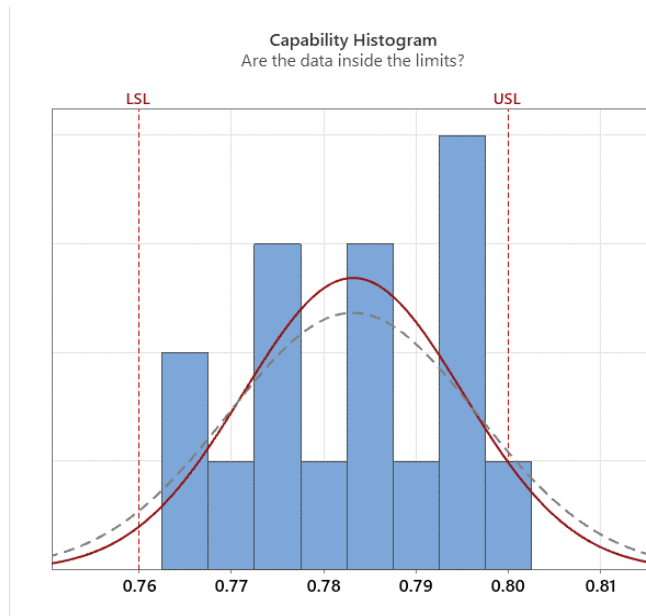**Figure 8.** Control chart of the burr width for App_02

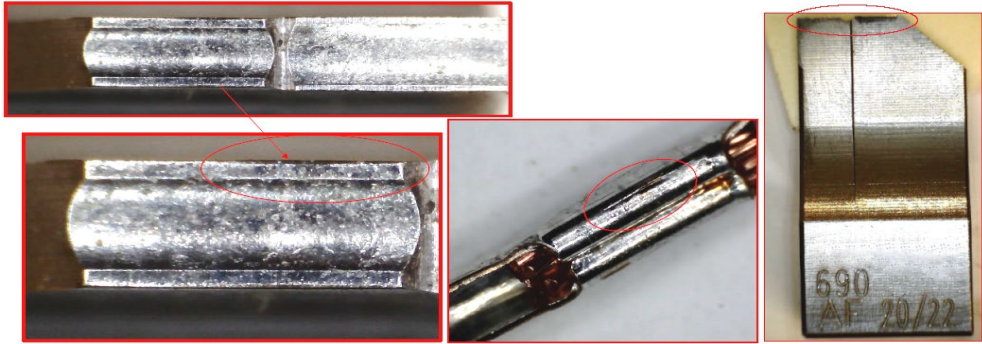**Figure 9.** Histogram analysis of crimp height for App_02

Figure 10. Damage on the anvil and the resulted crimp

The initial meter reading for App_02 stood at 2299978, while the final reading marked 2553490, reflecting a total of 253512 strokes. This cumulative stroke count, totaling 253512, surpassed the recommended spare parts exchange threshold of 200000 strokes, but not to the same extent as in case of App_01.

In light of our hypothesis that substantial variations in spare parts wear may exist among different crimping tools, the surplus of strokes, exceeding the recommended maintenance threshold, underscores the potential validity of our hypothesis. This outcome suggests that there may indeed be significant differences in wear patterns among these tools, necessitating a reevaluation of the existing internal maintenance instructions, while also stressing the need for further study in an attempt to be able to predict the lifespan of the spare parts.

4. Conclusions

Analyzing spare part longevity indicates potential for cost reduction in automotive production. While our initial findings are encouraging, it is evident that further testing is imperative to ascertain the complete lifecycle of these spare components.

Regular maintenance schedules and monitoring of spare part lifetimes can further enhance cost reduction efforts. A proactive approach in this regard is essential for enhancing production efficiency and cost-effectiveness.

Moreover, introducing a predictive model capable of simulating tests and extrapolating insights from empirical results represents a progressive avenue. Such a model could furnish valuable predictive tools, further refining cost-reduction strategies and potentially revolutionizing the management of spare parts in the automotive production process.

This study's significance lies in its immediate applicability within the automotive industry, where the delicate balance between cost reduction, quality maintenance, and operational efficiency is paramount. The potential implementation of these findings

could significantly impact production processes, leading to tangible reductions in costs and notable improvements in efficiency. However, the need for continued research is evident, beckoning further analyses and the development of predictive tools to refine maintenance strategies and deepen our understanding of spare parts management. Ultimately, this study not only identifies critical avenues for cost reduction but also lays the groundwork for the proactive, predictive methodologies that will shape the future of automotive production, establishing itself as a cornerstone in the ongoing evolution of the field.

References

1 Rachwan R., Abotaleb I., Elgazouli M., The Influence of Value Engineering and Sustainability Considerations on the Project Value, *Procedia Environmental Sciences,* 34, 2016, pp. 431-438, https://doi.org/10.1016/j.proenv.2016.04.038
2 Behncke F., Maisenbacher S., Maurer M., Extended Model for Integrated Value Engineering. *Procedia Computer Science*, 28, 2014, pp. 781-788, https://doi.org/10.1016/j.procs.2014.03.093
3 Mocellin K., Petitprez M., Experimental and Numerical Analysis of Electrical Contact Crimping to Predict Mechanical Strength, *Procedia Engineering*, 81, 2014, https://doi.org/10.1016/j.proeng.2014.10.274
4 Morgado L., Teixeira A., Sá, J. Pinto Ferreira L., Almeida F.D., Analysis and Development of a Failure Prediction Model for Electrical Terminals Used in the Automotive Industry, *Procedia Manufacturing,* 51, 2020, pp. 207-214, https://doi.org/10.1016/j.promfg.2020.10.030
5 Jongwuttanaruk K., Thavornwat C., Optimization of Mechanical Crimping in the Terminal Crimping Process Using a Response Surface Methodology, *Advances in Materials Science and Engineering*, Article ID 6508289, 2022, https://doi.org/10.1155/2022/6508289
6 Dragomir F., Manescu T., Gillich G.-R, Korka Z. Tufisi C., Influence of vibration and environmental factors on a crimped assembly resistivity, *Vibroengineering Procedia*, 51, 2023, pp. 173-178, https://doi.org/10.21595/vp.2023.23681
7 Castro T.A.M., Campilho R., Optimising a Specific Tool for Electrical Terminals Crimping Process, *Procedia Manufacturing*, 11, 2017, pp. 1438-1447, https://doi.org/10.1016/j.promfg.2017.07.274
8 SAE International, *Performance Specification for Cable-to-Terminal Electrical Crimps. SAE/USCAR-21,* 4th SAE International, U.S. and Canada, 2020. https://global.ihs.com/doc_detail.cfm?document_name=SAE%20USCAR %2D21&item_s_key=00407431.

Addresses:

- Ph.D. Stud. Eng. Dacian Ilca, Doctoral School of Engineering, Babeș-Bolyai University, Cluj-Napoca, Romania, Faculty of Engineering, Piața Traian Vuia, nr. 1-4, 320085, Reşiţa, Romania
  florin.dragomir@ubbcluj.com
- Assoc. Prof. PhD. Habil. Eng. Tiberiu Manescu, Doctoral School of Engineering, Babeș-Bolyai University, Cluj-Napoca, Romania, Department of Automation, Industrial Engineering, Textiles and Transportation, Aurel Vlaicu University, Bd. Revoluției 77, 310032, Arad, Romania
  manescu.tiberiu@gmail.com
  (*corresponding author*)
- Lect. Ph.D. Eng. Cristian Tufisi, Babeș-Bolyai University, Cluj-Napoca, Romania, Department of Engineering Science, Babeș-Bolyai University, Cluj-Napoca, Babeș-Bolyai University, Faculty of Engineering, Piața Traian Vuia, nr. 1-4, 320085, Reşiţa, Romania, tufisi.cristian@ubbcluj.ro

Essential biomechanical aspects in athletics

Daniel-Mihai Amariei, Zeno-Iosif Praisach*, Zoltan Iosif Korka, Andrade-Ionuț Bichescu

Abstract. *The aim of this paper is to present theoretical aspects of the study of biomechanics in athletics, which is essential for performance optimization, injury prevention, and improvement of athletes' capabilities. This study contains various research directions in athlete biomechanics as well as biodynamic modeling and simulation in athletics. Finally, aspects of athlete training design and optimization are presented, which are essential for tailoring training programs to the individual needs and goals of athletes.*

Keywords: *biomechanical model, optimization, performance, evaluation, objectives*

1. Introduction

Studies in the field of biomechanics have highlighted significant differences in performance between trained and untrained subjects regarding the biomechanical aspects of athletic movement. Here are some observed differences:

- *Movement Efficiency*: Trained athletes generally exhibit greater efficiency in their movements compared to untrained subjects. This is primarily due to the development of better techniques, improved muscle coordination, and the ability to generate force and power optimally [8].
- *Kinematics and Kinetics of Movement*: Trained subjects often demonstrate more precise and controlled movement patterns compared to untrained individuals. This can be reflected in more appropriate joint angles, better limb alignments, and more efficient force distributions [12].
- *Muscle Power and Strength*: Trained athletes generally possess greater muscle power and strength compared to untrained subjects. This is due to specific muscle development and neuromuscular adaptations that occur through training.

- **Muscular Endurance**: Trained athletes often exhibit superior muscular endurance compared to untrained individuals. This allows them to maintain performance and movement efficiency during intense and prolonged sports activities.
- **Stability and Motor Control**: Regular training can contribute to improving the stability and motor control of athletes.

These aspects are essential for injury prevention and optimal performance in athletic movements. It is important to note that individual variations and differences in athletes' training can influence the performance differences observed in studies. Additionally, the level of training and sports experience can vary among different athletes and sports, contributing to variations in the biomechanics of athletic movements [2].

Overall, regular and specialized training plays a crucial role in the development of athletes' biomechanical capabilities, enabling them to achieve superior performance and maximize their potential in their sporting activities.

Purpose of the Study:

The purpose of this study is to conduct a comprehensive theoretical review of the significance of biomechanics in the context of sports. This review aims to underscore the direct applications of biomechanical principles in enhancing sports performance, mitigating the risk of injuries, and fostering the development of athletes' skills."

2. Research Directions in Athlete Biomechanics

In the field of athletic biomechanics, there are several research directions that can contribute to understanding and enhancing athletic performance. Here are some relevant research directions in athlete biomechanics:

- **Analysis and Technique Optimization**: Research can be focused on analyzing and understanding the specific techniques of each sport discipline. Studies can examine key factors influencing performance, such as proper body alignment, muscle coordination, applied force, and moment, to identify ways to optimize technique [8].
- **Force and Power Generation Mechanisms**: Research can focus on understanding the mechanisms of force and power generation in various athletic movements. These studies can explore how muscular characteristics and neuromuscular coordination contribute to the development of force and power in specific sports activities [12].
- **Injury Prevention and Rehabilitation**: Biomechanics can play a significant role in the prevention and rehabilitation of athlete injuries. Research can examine biomechanical risk factors for different types of injuries, such as running and jumping biomechanics, and identify interventions to minimize the risk of injury and accelerate recovery [2].

- **Adaptation and Individual Performance**: Research can explore individual variations in athlete biomechanics and how they influence sports performance. This may include studies on gender differences, age differences, or variations based on training level and sports experience.
- **Innovative Measurement and Analysis Technologies**: In recent years, new technologies and measurement methods in biomechanics have emerged, such as the Opto Jump system, 3D tracking systems, computerized image analysis, and numerical simulations. Research can explore the use of these technologies to obtain more precise data and investigate more detailed aspects of athlete biomechanics [1].

These are just a few examples of research directions in athlete biomechanics. With technological advancements and progress in the field of biomechanics, there are ongoing opportunities for research and innovation in understanding and optimizing athletic performance [10].

3. Biodynamic Modeling and Simulation in Athletics

Biodynamic modeling and simulation in athletics is an approach that uses mathematical models and computer simulations to understand and evaluate the biomechanical behavior of athletes during sports activities. This method provides a detailed perspective on forces, moments, and interactions between body segments and musculoskeletal systems during athletic motion. Key aspects of biodynamic modeling and simulation in athletics include:

- **Development of Biomechanical Models**: Biodynamic modeling involves developing mathematical models that describe the structure and behavior of the musculoskeletal systems involved in athletic movement. These models may include information about the geometry and mechanical properties of body segments, muscles, tendons, and joints [9].
- **Model Validation**: To ensure the accuracy and validity of models, they must be validated by comparing their results with experimental data collected in real or laboratory conditions. This involves using measurement technologies such as 3D tracking systems, force plates, or EMG systems to collect reference data [12].
- **Athletic Motion Simulation**: Using the developed models and validated data, computerized simulations of athletic motion can be created. These simulations can reproduce an athlete's specific movements and provide detailed information about the forces, moments, and muscle demands involved in that motion.
- **Analysis and Interpretation of Results**: Biodynamic simulations can provide valuable information about the performance and behavior of athletes in different

situations. By analyzing the results, factors influencing performance can be evaluated, technical deficiencies can be identified, and strategies for optimizing athletic performance can be developed [6].

- **_Training Design and Optimization_**: Biodynamic modeling and simulation can be used to optimize training programs. By simulating different scenarios and interventions, the effects of training on performance can be evaluated, and personalized strategies can be developed for each athlete.

Biodynamic modeling and simulation in athletics offer a complementary and detailed perspective on biomechanics and athletic performance. It can contribute to improving technique, optimizing performance, and preventing injuries in athletics [4].

4. Development of Biomechanical Models

The development of biomechanical models is a complex and interdisciplinary process that involves collecting data, identifying the structure and behavior of the biological system, and using mathematical and technological methods to create a representative model. The steps involved in developing biomechanical models are:

- **_Defining Objectives_**: The first step in developing a biomechanical model is to establish objectives and research questions. It is important to clarify what information is desired and how the resulting model will be used [8].
- **_Data Collection:_** An essential aspect of developing biomechanical models is collecting relevant data. This can include measurements from human subjects, data from existing literature, information about the mechanical properties of tissues, medical images, and more. The data should be precise, valid, and representative of the biological system being analyzed [11].
- **_Identification and Description of Components_**: Biomechanical modeling involves identifying and describing the key components of the biological system under study. This may include the structure and geometry of body segments, mechanical properties of tissues (such as stiffness and elasticity), and muscular and joint characteristics.
- **_Formulation of Mathematical Relationships:_** Biomechanical modeling involves formulating mathematical relationships that describe the behavior of the biological system. These may include equations of motion, equilibrium equations, relationships between force and motion, force and muscle length, and so on. These relationships are based on relevant physical and biomechanical principles [15].
- **_Model Implementation_**: The biomechanical model is implemented in a computational environment, such as specialized software or simulation platforms. Here, the collected data, mathematical relationships, and other relevant parameters are entered to create a functional model [11].

- *Validation and Evaluation of the Model*: Validation of the biomechanical model involves comparing the model's results with experimental data or real observations. This is a crucial step to ensure that the model accurately reproduces the behavior of the biological system and provides correct and valid results [3].
- *Use and Refinement of the Model*: The biomechanical model can be used to investigate specific research questions, simulate different scenarios, or optimize athletic performance. Depending on the results obtained, the model may need refinement and improvement to provide more accurate and relevant results.

5. Model Validation

Model validation is an important process to ensure that developed models are representative and provide accurate and credible results. Validation involves comparing the results obtained from models with experimental data or real observations to check their accuracy and reliability. Basic information about model validation includes:

- *Experimental Data Collection*: To validate a biomechanical model, it is necessary to collect relevant experimental data. This data may include measurements from human subjects, data from existing literature, or results from laboratory experiments. It is essential that the data is collected under controlled conditions and accurately represents the behavior of the biological system being studied [8].
- *Comparison of Model Results with Experimental Data*: After developing the model, the results obtained from it are compared with relevant experimental data. This involves analyzing both numerical values and trends and general characteristics of motion or biomechanical behavior. The comparison can be done using statistical methods such as root mean square error (RMSE), correlation coefficient, or cross-validation tests [9].
- *Sensitivity to Variations and Uncertainties*: Model validation must take into account the sensitivity of the model to variations and uncertainties in experimental data or model parameters. Sensitivity analysis can identify factors that may influence the results and help improve the accuracy and robustness of the model [12].
- *External and Internal Validation*: Validation of biomechanical models can involve both external validation, where model results are compared with experimental data from other sources or studies, and internal validation, where model results are compared with experimental data from the same dataset or subjects.

- *Reassessment and Model Refinement*: Depending on the results obtained during the validation process, it may be necessary to reassess and refine the model. This may involve adjusting model parameters, revising mathematical relationships, or adding additional factors to improve the accuracy and validity of the model.

Model validation is a critical step in ensuring that biomechanical models provide reliable and trustworthy results, which can be used for research, analysis, and decision-making in various fields, including sports biomechanics [10].

6. Athletic Motion Simulation

Athletic motion simulation is the process of using mathematical models and computer simulations to recreate and analyze the movements and biomechanical behavior of athletes during sports activities. This approach provides an opportunity to better understand the mechanisms and factors influencing athletes' performance and can help optimize technique, training, and injury prevention. Key aspects of athletic motion simulation include:

- *Biomechanical Modeling:* Athletic motion simulation begins with the development of a biomechanical model representing the biological system involved. This model may include the structure and geometry of body segments, mechanical properties of tissues, muscle and joint characteristics, and other relevant factors [9].
- *Data Input and Parameters:* Simulation involves entering the collected data and parameters into the biomechanical model. This data may include information about initial motion, muscle properties, neuromuscular coordination, external forces, and other factors influencing athletic motion [8].
- *Numerical Simulation:* Using numerical methods and algorithms, the biomechanical model is simulated in a computational environment, such as specialized software. During simulation, values and mathematical relationships are evaluated at each moment of motion to determine the evolution and behavior of the biomechanical system [2].
- *Analysis of Results:* After completing the simulation, the obtained results are analyzed and interpreted. These results can include information about trajectories, joint angles, forces, joint moments, load distribution, and other parameters relevant to athletic motion. The analysis of results can provide insights into factors contributing to performance, efficiency, and the risk of injury [12].

- ***Optimization and Performance Improvement:*** Athletic motion simulation can be used to optimize and enhance athletes' performance. Based on the results, technical deficiencies can be identified, personalized training strategies can be developed, and variations and interventions can be explored to maximize athletes' performance [10].

7. Training Design and Optimization

Training design and optimization involve the process of developing training programs that maximize athletes' performance and help them achieve their individual and performance goals. Here are some key aspects of training design and optimization:

- ***Initial Athlete Assessment***: The process of designing training starts with an initial assessment of athletes, including evaluations of physical capacities, technical skills, and sports performance. This assessment helps identify athletes' strengths and weaknesses and sets realistic and personalized goals [9].
- ***Goal Setting***: Based on the initial assessment, specific goals are set for each athlete. These goals can include improving strength, power, endurance, speed, or sport-specific techniques. Goals should be SMART (specific, measurable, attainable, relevant, and time-bound) [5].
- ***Training Planning:*** Training planning involves structuring the volume and intensity of training sessions. It considers principles of adaptation and progression, exercise variation, and recovery periods. Training can be planned for the short term (weeks) and long term (months/years), taking into account competitions and rest periods [7].
- ***Individualized Training***: Each athlete has unique needs and capabilities. Training design should consider these differences and be tailored to individual needs and goals. This may involve modifying the volume and intensity, choosing exercises and training methods, and considering physical, technical, and psychological aspects [13].
- ***Monitoring and Adjustment***: Training needs regular monitoring to assess progress and the effectiveness of the training program. This may involve measuring athletes' performance, evaluating established goals, and providing continuous feedback based on progress and adjusting training according to the results.
- ***Integration of Recovery Factors***: Optimizing training goes beyond the training sessions themselves. Attention should be given to recovery factors such as rest, proper nutrition, sleep, stress management, and active recovery techniques. These aspects contribute to recovery, regeneration, and the avoidance of overtraining.

Training design and optimization are crucial for improving athletes' performance, and they require a personalized and goal-oriented approach. The design and monitoring of training programs help athletes reach their full potential while minimizing the risk of injury and overexertion [4].

The process of selecting articles for this review of biomechanics in sports involved the following steps:

I conducted a systematic search across various academic databases, including PubMed, Google Scholar, Web of Science, and sport science journals. These databases were chosen for their comprehensive coverage of relevant literature.

Articles were considered for inclusion if they met the following criteria:

Published within the last 10 years (between 2013 and 2023) to ensure relevance.

Relevant to the study's objectives, specifically addressing biomechanics in sports and its applications in performance optimization, injury prevention, or athlete skill development.

Selected articles from the initial screening phase underwent a comprehensive examination of their full texts. We assessed them for relevance, methodology, and their potential contributions to the study's objectives.

In addition to the database search, we reviewed the reference lists of selected articles to identify additional sources that might have been overlooked in the initial search.

After a thorough evaluation, the final selection of articles was made based on their alignment with the study's focus and their potential to enhance the theoretical review of biomechanics in sports.

An assessment of each article's quality, methodology, data sources, and potential biases was conducted. This quality assessment was a critical part of the final selection process.

By following this systematic methodology for article selection, my aim was to ensure the integrity and comprehensiveness of the review, providing readers with a well-rounded understanding of the role of biomechanics in sports.

8. Conclusion

In conclusion, the study of biomechanics in athletics is essential for optimizing performance, preventing injuries, and enhancing athletes' capabilities.

It encompasses various research directions, such as technique optimization, force and power generation, injury prevention, and the use of innovative measurement technologies. The development of biomechanical models and their validation is

crucial for ensuring the accuracy and reliability of the results obtained. Athletic motion simulation offers a detailed perspective on athletes' movements, which can be used to analyze and optimize performance. Finally, training design and optimization are essential for tailoring training programs to individual athletes' needs and goals. The field of athlete biomechanics continues to evolve with advancements in technology and research, offering new opportunities to improve athletic performance and overall well-being. Understanding and applying biomechanical principles in sports not only benefits athletes but also contributes to the advancement of sports science as a whole.

References

1 Baechle T.R.. Earle, R.W., *Essentials of Strength Training and Conditioning*, Human Kinetics, 2008.
2 Bartlett R., *Introduction to Sports Biomechanics: Analysing Human Movement Patterns*. Routledge, 2007.
3 Bartlett R.M., *Introduction to Sports Biomechanics: Analysing Human Movement Patterns*, Routledge, 2017.
4 Bompa T.O., Haff, G.G., *Periodization: Theory and Methodology of Training*, *Human Kinetics*, 2009.
5 Cavanagh P.R., Lafortune M.A., Ground reaction forces in distance running. *Journal of Biomechanics*, 13(5), 1980, 397-406.
6 Zatsiorsky V.M., Kraemer W.J., *Science and Practice of Strength Training*, Human Kinetics, 2006.
7 Dapena J., *Introduction to Sports Biomechanics: Analysing Human Movement Patterns*, Routledge, 2010.
8 Enoka R.M., *Neuromechanics of human movement*, Human Kinetics, 2008.
9 Enoka R.M., *Neuromechanics of Human Movement*. Human Kinetics, 2015.
10 Fleck S.J., Kraemer W.J., *Designing Resistance Training Programs*. Human Kinetics, 2014.
11 Hamill J., Knutzen K.M., Derrick T.R*., Biomechanical Basis of Human Movement*, Lippincott Williams &Wilkins, 2014.
12 Winter D.A., *Biomechanics and Motor Control of Human Movement*, Ed. John Wiley & Sons, SUA, 2009.
13 Hay J.G., *The Biomechanics of Sports Techniques*. Prentice Hall, 1993.
14 Hay J. G., *The biomechanics of sports techniques*, Routledge, 2016.
15 Zatsiorsky V.M., Kraemer W.J., *Biomechanics in sport: Performance enhancement and injury prevention*, John Wiley & Sons, 2016.

Addresses:

- Phd. Daniel-Mihai Amariei, Doctoral School of Engineering, Babeș-Bolyai University, Cluj-Napoca, Romania, Faculty of Engineering, Piața Traian Vuia, nr. 1-4, 320085, Reşiţa, Romania
  daniel.amariei@ubbcluj.ro
- Lect. Dr. Eng. Habil. Zeno-Iosif Praisach, Department of Engineering Science, Babeș-Bolyai University, Cluj-Napoca, Romania, Faculty of Engineering, Piața Traian Vuia, nr. 1-4, 320085, Reşiţa, Romania,
  zeno.praisach@ubbcluj.ro
  (*corresponding author)
- Assoc. Prof. Dr. Eng. Zoltan Iosif Korka, Department of Engineering Science, Babeș-Bolyai University Cluj-Napoca, Romania, Faculty of Engineering, Piața Traian Vuia, nr. 1-4, 320085, Reşiţa, Romania,
  zoltan.korka@ubbcluj.ro
- Assoc. Prof. Dr. Andrade-Ionuț Bichescu, Babeș-Bolyai University, Cluj-Napoca, Romania, Faculty of Physical Education and Sport,
  andrade.bichescu@ubbcluj.ro

Table of content